CRANFIELD UNIVERSITY

C TYDEMAN

THE FURTHER ASSESSMENT OF A HANDHELD RAMAN SPECTROSCOPY PROBE FOR THE INTRAOPERATIVE DIAGNOSIS OF AXILLARY LYMPH NODES IN BREAST CANCER

SCHOOL OF HEALTH

MSc by Research

MSc THESIS

Academic year: 2011-2012

Academic Supervisor: Professor N Stone

Clinical Supervisors: Mr J Bristol; Mr C Chan

September 2012

CRANFIELD UNIVERSITY

SCHOOL OF HEALTH

MSc by Research

MSc THESIS

Academic year: 2011-2012

C TYDEMAN

The further assessment of a handheld Raman spectroscopy probe for the intraoperative diagnosis of axillary lymph nodes in breast cancer

Academic Supervisor: Professor N Stone

Clinical Supervisors: Mr J Bristol; Mr C Chan

September 2012

This thesis is submitted in partial fulfilment of the requirements for the degree of Master of Science

ABSTRACT

Axillary sentinel lymph node biopsy plays an important role in breast cancer management in determining further surgical and medical treatment options. Intraoperative assessment of the sentinel lymph node might allow immediate axillary surgery, which would incur benefits to both the patient and healthcare trusts. A handheld Raman spectroscopy probe has already been shown to be a comparable option for intraoperative assessment through previous published and unpublished studies, delivering a sensitivity of up to 92% and specificity of up to 99%.

This research aims to define further the role of the hand-held Raman spectroscopy probe as an accurate, rapid and non-destructive technique for intra-operative axillary node assessment, making it a strong competitor in the clinical market. It also looks to improve the sensitivity of the probe by altering the methodology used in previous studies.

122 lymph node halves were collected intraoperatively from 37 patients diagnosed with breast cancer and spectra measured using a commercially available handheld Raman spectroscopy probe. Spectra were then fed into a specialist software programme and analysed using principal component fed linear discriminant analysis trained by histopathology results.

A “2 group” training model defining the probe’s ability to distinguish between benign and malignant tissue produced an overall performance of 86.4%, with a sensitivity of 71% and specificity of 91%.

The results were not as impressive as previous studies. This was possibly due to a broken probe, leading to four different phases of measurements (original probe/failing probe/temporary replacement/mended probe). Secondly a smaller, less balanced data set, in terms of spectra per pathology group, was collected and there appeared to be more fluorescence in some of the data which may have originated from varying blue dye injection protocols. However, that said further research using a robust, high specification system may help establish its role as a reliable assessment tool intraoperatively as well as a non-invasive means of assessing lymph nodes in the initial assessment clinic.

ACKNOWLEDGEMENTS

I would like to thank my supervisors for their ongoing support and contributions to this work - Professor Nick Stone for his continued help, insights and experience; Mr James Bristol and Mr Charlie Chan (Consultant General & Breast Surgeons) for their patience, enthusiasm and guidance in the operating theatre.

This work was funded by the Bupa Foundation, the medical research charity, to which I am most grateful. I am also grateful to Gloucestershire NHS Foundation Trust for facilitating my research.

CONTENTS

LIST OF FIGURES

LIST OF TABLES

CHAPTER 1 INTRODUCTION

1.1 Breast Cancer in the UK

Breast Cancer is the most common cancer in the UK. In 2008 alone, there were 48,034 new cases diagnosed, accounting for 31% of all cases of cancer in women (Office for National Statistics 2010).

The disease itself is age-related. Nearly half of the women diagnosed are within the 50-69 year old age group. However, of note, it is the second most commonly diagnosed cancer in women under 35.

With respect to mortality, breast cancer is the second most common cause of cancer death in women following lung cancer. Just over 10,000 women died from the disease in England in 2008 which is equivalent to a rate of 26 deaths per 100,000 women (Office for National Statistics 2010).

However, although incidence rates for breast cancer increased by more than 85% between 1971 and 2008, mortality rates fell by 33%. Survival rates are significantly higher than those for other major cancers in women. Five-year survival was 83% for women in England

diagnosed in 2003-07 and followed up to the end of 2008. In fact, almost 2/3 of women diagnosed with breast cancer survive beyond 20 years (Office for National Statistics 2010).

These impressive figures are a result of both earlier detection through the national screening programme and improved management of the disease.

1.2 Breast Cancer Management

In 2009, the Association of Breast Surgery presented the basis of "gold standard" breast cancer management through a set of guidelines (Association of Breast Surgery 2009) to support these improvements. The guidelines are divided into a number of categories:

1) Multidisciplinary care
2) Diagnostics
3) Treatment planning and patient communication
4) Organisation of Breast Cancer Surgical Services
5) Surgery for Invasive Breast Cancer
6) Axillary Node Management in Invasive Breast cancer
7) Surgical management of DCIS
8) Surgery for LCIS

9) Breast Reconstruction

10) Peri- and post-operative care

11) Adjuvant treatment

12) Clinical follow-up

1.3 Management of axillary lymph nodes in breast cancer

This research will be concentrating on axillary node management in invasive breast cancer. The guidelines above suggest that the presence of node metastases is the most powerful prognostic determinant in primary operable breast cancer. All patients in this group should therefore have axillary staging and treatment as appropriate.

In some cases, pre-operative axillary node assessment with ultrasound and fine needle aspirate (FNA) can yield a diagnosis of involved nodes. These patients will either go straight to axillary clearance, retrieving at least 10 nodes, in their primary operation or will have axillary radiotherapy post-operatively.

In most cases, however, sentinel node biopsy has become the standard approach for staging, providing accurate axillary assessment with good sensitivity and specificity rates. The

histological status of the sentinel node has been shown to reflect the overall status of the axilla in over 97% of cases (Veronesi *et al* 1997).

Sentinel lymph node biopsy involves injection of blue dye and/or a radio-isotope into the ipsilateral breast to indicate the first few axillary nodes draining the breast. These are removed via a small axillary incision and sent for histopathological assessment. Any evidence of macrometastases or indeed micrometastases should point towards further axillary treatment in the form of radiotherapy or axillary clearance at a later date in addition to adjuvant systemic therapy.

Unfortunately, both axillary radiotherapy and clearance leads to significant comorbidity. Symptoms include lymphoedema, reduced mobility and recurrent infections in the ipsilateral arm. Therefore it should only be performed if necessary to the patient.

1.3.1 The future of axillary lymph node management

In 2011, a randomised trial of axillary node dissection in women with clinical T1-2 breast cancer with positive sentinel nodes was carried out in the United States over 115 treatment centres (Giuliano *et al* 2011). The results demonstrated that among this patient group breast conservation surgery and systemic therapy with sentinel lymph node dissection alone inferred no less survival benefit than those undergoing complete axillary clearance. It

should be emphasised that these results apply only to patients meeting the very specific criteria of the study. The study was also restricted to 891 of the planned 1900 patients. So far, clinical practice in the UK has remained unchanged but the potential effects it could have on surgical guidelines, if further evidence is documented, is enormous.

1.4 Intraoperative axillary node staging

The introduction of axillary sentinel node biopsy as a standard practice has welcomed the challenge of intra-operative staging of the axillary nodes. Traditionally, the sentinel nodes excised during the initial operation for the primary breast tumour are sent away for histological assessment.

Unfortunately, this requires the patient to wait before finding out if a full clearance or radiotherapy is needed. Psychological stress, delay in any adjuvant treatment, and increased cost implications of further surgery and hospital admission are all significant concerns as a result (Layfield *et al* 2011).

Intra-operative staging would offer the patient definitive treatment of the axilla in the initial operation, thus potentially resolving these issues. However, in order to be a gold standard treatment, both specificity and sensitivity must remain high. False positive results would

lead to unnecessary axillary clearance, resulting in significant comorbidity as outlined above. Meanwhile, false negative results, whilst not deleterious to the patient, would leave us with a system where results have to be double-checked, thus adding to costs.

There are a number of techniques being studied to look at intraoperative lymph node assessment.

1.4.1 Histological techniques

Intraoperative frozen section analysis of sentinel lymph node biopsies is currently the most commonly used technique. Its reported sensitivity ranges from 57% to 74% whilst specificity ranges between 99-100% (Layfield *et al* 2011).

Unfortunately, the process is expensive, time poor and labour intensive. It relies on a dedicated histopathologist being available. Frozen sections themselves can carry freeze artifacts and the histological morphology is poorer than paraffin sections which could attribute to lower sensitivities. Furthermore, the tissue, once frozen, is lost and this can lead to concerns about missing micrometastases and understaging lymph nodes.

1.4.2 Cytological techniques

Touch imprint cytology involves the cut surface of a sentinel lymph node being pressed or scraped against a glass slide. This is subsequently stained and examined under a microscope by a histopathologist. A meta-analysis of 31 articles by Tew (Tew *et al* 2005) estimated sensitivity levels at 63% and specificity levels at 98-99%. Leaving micrometastases out of the equation the sensitivity rises to 81% for macrometastases alone. This is due to the smaller amount of cellular tissue examined and the size of micrometastases themselves.

Further studies have found that the sensitivity of imprint cytology also varied according to the type of invasive breast cancer (Cox *et al* 2005). Invasive lobular cancer has cells which are poorly cohesive and tend to resemble lymphoid cells. Sensitivity for lobular carcinoma metastases was therefore 38.7% compared with 55.5% for ductal type.

Whilst cytology is certainly faster and cheaper than frozen section, it still requires the presence of a histopathologist. Its sensitivities may well be improved by increased sampling as well as the use of immunocytochemistry. The latter has been incorporated in various studies and advocated as a means of improving diagnosis in invasive lobular carcinoma (Leikola *et al* 2005) as well as detection of micrometastases (Salem *et al* 2006). Despite

increased sampling and immunostaining, tissue is preserved for further histological assessment post-operatively.

1.4.3 Molecular techniques

Molecular techniques to assess the sentinel lymph node look for the presence of marker genetic material. In this way, the techniques are essentially assessing the whole lymph node rather than just sections, potentially removing the danger of sampling error.

Quantitative Reverse Transcriptase-polymerase chain reaction (qRT-PCR) differentiates between high levels of marker mRNA in tumour cells and the lower "expected" levels in non-cancerous tissue. Unfortunately there is no single gene yet identified which is expressed universally in cancer cells.

In 2005, Backus therefore used a combination of widely expressed markers MGB1 and CK-19. They managed to achieve sensitivity of 91% and specificity of 97% in laboratory conditions (Backus *et al* 2005).

The first commercially available assay based on this technology and using these two markers was the Genesearch^{TM} Breast Lymph Node (BLN) Assay (Veridex, Warren, New Jersey, USA).

Blumencranz (Blumencranz *et al* 2007) carried out a prospective study of 416 patients where positive or negative BLN Assay results, generated from fresh 2-mm node slabs, were compared with results from conventional histological evaluation of adjacent fixed tissue slabs. The assay detected 98% of metastases greater than 2 mm and 88% of metastasis greater than 0.2 mm. Micrometastases were less frequently detected (57%) and assay positive results in nodes found negative by histology were rare (4%). This concluded that the BLN Assay was properly calibrated for use as a stand- alone intraoperative molecular test.

However, despite this, the product was withdrawn from the market due to low demand. The Wall Street Journal attributed this to high set up costs, concerns about lower specificity rates than frozen section analysis as well as logistical difficulties (Loftus *et al* 2010).

The reduced specificity could be a result of contamination from the primary breast tissue during excision. Advocates of the technique have also argued that the discrepancies in specificity may result from the inability to directly compare histology of the same tissue

due to homogenisation of the tissue for PCR. The metastatic deposit may have been entirely within the sample taken. Indeed, further analysis of lysate from BLN-positive and histology-negative lymph nodes with additional molecular markers have supported the presence of metastatic material in up to 76% of these samples (Blumencranz *et al* 2007).

An alternative to qRT-PCR is Reverse Transcriptase loop-mediated isothermal amplification (RT-LAMP). Similarly, it uses reverse transcriptase to convert mRNA to cDNA. However, it then uses 6 primers specific to that cDNA target to cause looping of the DNA during amplification which results in the release of a by-product, pyrophosphate. Pyrophosphate binds to magnesium causing precipitation. The extent of precipitation is used to quantify the amount of target gene present.

Studies using this technique have described specificities between 89 to 97.1% with sensitivities between 92.9 to 98.1% (Layfield *et al* 2011).

1.4.4 Raman Spectroscopy

Recent studies using a hand held Raman spectroscopy probe have proposed a further tool which is a potentially efficient method of diagnosing metastases in axillary lymph nodes. Its properties are comparable to those above and this will be explored further. The theory behind this technique will be described in Chapter 3 and 4.

1.5 Thesis Objectives

This study aims to address the following proposals in relation to Raman Spectroscopy as a means of accurately assessing lymph nodes intraoperatively:

- Use of a hand-held Raman Spectroscopy probe in theatre is an accurate, rapid and non-destructive technique for intraoperative axillary node assessment.

- The sensitivity of the Raman Spectroscopy probe is improved by recording spectra at more than one site on the lymph node.

- The Raman Spectroscopy probe has characteristics comparable to histopathology such that it is a strong competitor in the clinical market for intraoperative lymph node assessment.

CHAPTER 2 THE BREAST AND BREAST CANCER

2.1 The Breast and Axilla

2.1.1 Anatomy

The breasts, also known as mammary glands, are considered to be highly modified apocrine sweat glands. In both sexes, the breasts follow a similar developmental course until puberty. At this stage the female breasts develop under the influence of pituitary, ovarian and other hormones. From puberty to the menopause, the breast tissue undergoes cyclical changes controlled by hormones of the ovarian cycle. After menopause, the breasts undergo gradual atrophy and involution.

The breast consists of glandular tissue and fat embedded in the superficial fascia of the anterior chest wall. Although the size and shape of the female breast can vary, its base is constant and overlies three muscles – *pectoralis major*, *serratus anterior* and *rectus abdominis*. In the adult female, the base is roughly circular and extends between the second and sixth ribs. Medially it overlies the lateral border of the sternum. Part of the breast also extends upwards and laterally, reaching the anterior fold of the axilla, forming the axillary tail.

The breast's structural architecture is created by the fatty tissue divided by *Cooper's suspensary ligaments*. Opening on to the surface of the nipple are 20 or so *lactiferous ducts*. Each of these ducts drains milk from different segments (*lobes*) of the breast. At the end of each duct are a number of *lobules* that consist of multiple *acini*. These are the milk-producing glands, which are hormone dependent. *Terminal ducts* connect the acini to the mammary ducts. (Figure 2.1)

Figure 2.1 Breast Anatomy (www.breastdiagnostic.com; 03/09/2012)

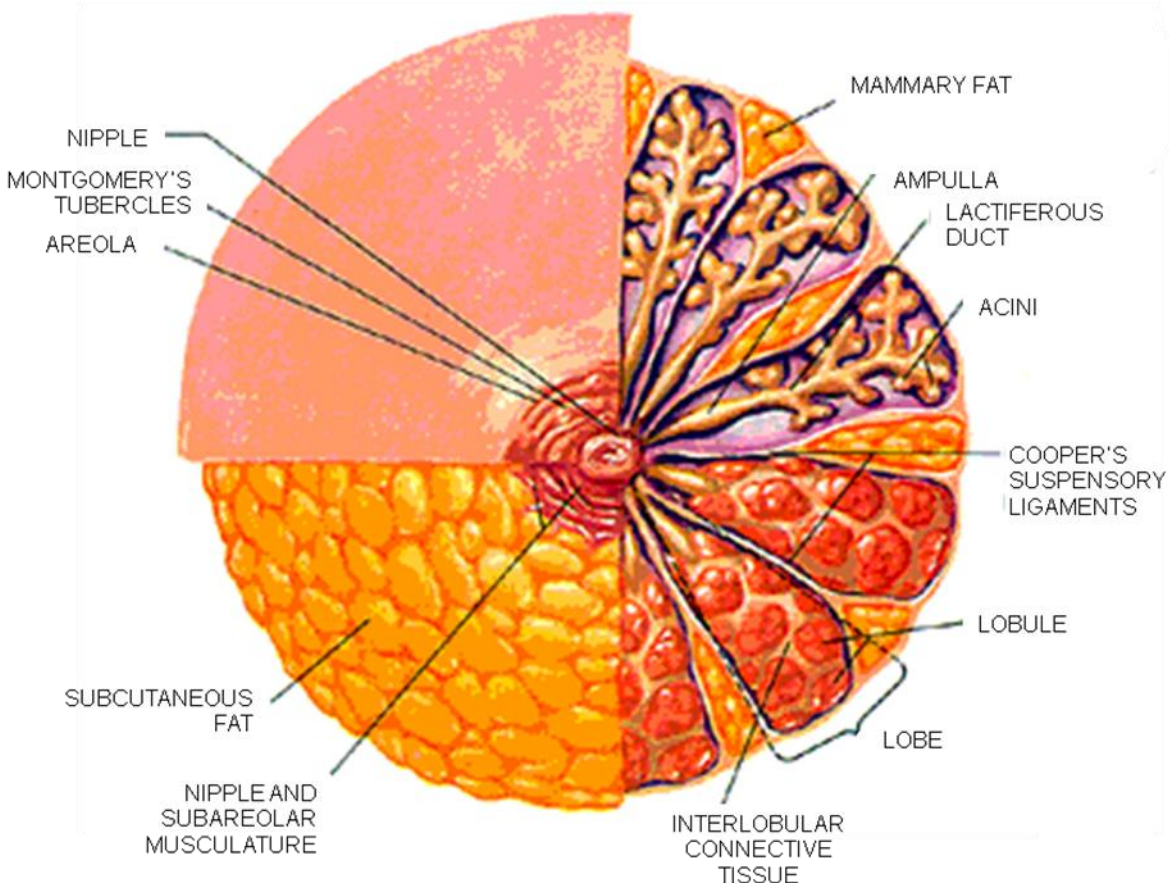

The axilla (Figure 2.2) is the space between the root of the upper limb and the chest wall. It is traversed by the main vessels and nerves which pass between the upper limb and root of neck. Its shape can be thought of as a pyramid with a narrow apex superiorly and a broad base with three walls. The structures at risk of iatrogenic damage during a surgical axillary dissection are:

- Axillary vein
- Long thoracic nerve – supplies *serratus anterior*
- Thoracodorsal nerve – supplies *latissimus dorsi*
- Intercostal brachial nerve – supplies sensation for inferior aspect of the arm and posterior aspect of axilla itself

Figure 2.2 The Axilla (www.breastdiseases.com; 03/09/2012)

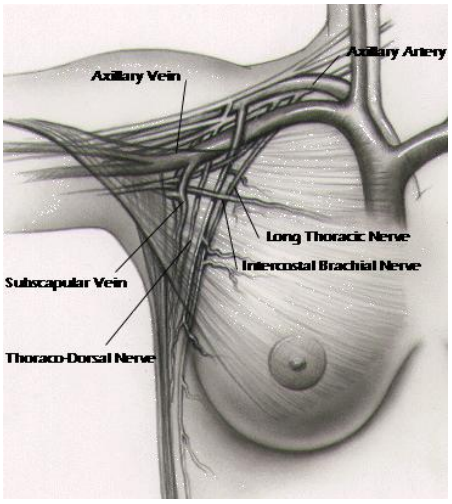

2.1.2 Blood Supply

The breast receives blood from branches of arteries supplying the deeper structures of the chest wall (*internal thoracic artery* and the *second, third and fourth intercostal arteries*) as well as the *lateral thoracic* and *thoracoacromial arteries*, which are branches of the *axillary artery*.

2.1.3 Lymph Drainage

The lymphatic system is part of the body's immune system that carries lymph from tissues back towards the heart and ultimately back into circulation via a network of conduits called lymphatic vessels. The system has a number of functions which include removal of interstitial fluid from tissues; absorption and transport of fats from bloodstream (chyle); transport of white blood cells to and from lymph nodes; assisting in the body's immune response when stimulated.

Due to its proximity to many tissues within the body, it is also responsible for carrying cancer cells away from a primary site of neoplastic growth, a process called metastasis.

The breast's lymphatic system drains into two anatomical sets of lymph nodes - 75% of lymph goes to axillary nodes whilst the rest goes to the internal mammary nodes near the centre of the chest. (Figure 2.3)

Figure 2.3 Lymphatic Drainage of the breast (www.breastdiseases.com; 03/09/2012)

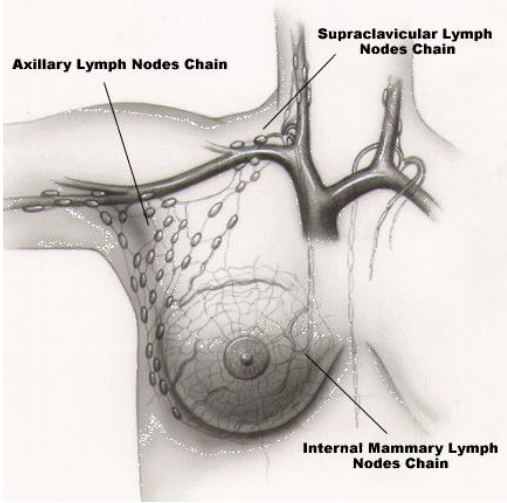

2.2 Lymph Nodes

Lymph nodes tend to occur in groups. The main ones are found where the lymphatics converge to form larger trunks – neck; axillae (as above); groins; lung hila and para-aortic areas.

The cells making up the lymph node can be divided into three functional types (Burkitt 1993):

- Lymphoid cells – Lymphocytes of all types and their derivatives.
- Immunological accessory cells – macrophages and other phagocytic antigen processing and presenting cells.
- Stromal cells – lymphatic and vascular endothelial cells and fibroblasts which are responsible for the structural framework of the lymph node.

Macroscopically, a lymph node is a small bean-shaped organ. Whilst inactive, it is only a few millimetres long but this increases in size when stimulated to mount an immunological response.

Microscopically, the outer part of the lymph node is cell-rich and is known as the *cortex*. The central area is less cellular and is called the *medulla*. Encapsulating the lymph node is dense collagenous tissue. From here *trabeculae* extend into the substance of the node.

Afferent lymphatic vessels branch outside the node then pierce this capsule to drain lymph into a narrow space called the *subcapsular sinus* which extends around and beneath the surface. From here, *cortical sinuses* pass towards the medulla through the cortex.

Within the medulla itself, the *medullary sinuses*, a network of broad interconnected lymphatic channels converge on the *hilum*. Lymph drains from here into the *efferent lymphatic vessels* (Figure 2.4).

Figure 2.4 Lymph Node (Burkitt 1993)

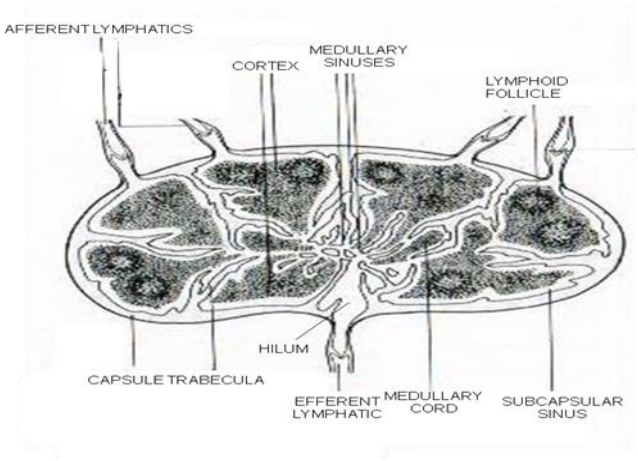

2.3 Breast Cancer

Breast cancer originates from breast tissue, usually either in the ducts or lobules. It can be classified according to its histological types as well as the site at which it originates.

2.3.1 Carcinoma-in-situ

The term *carcinoma-in-situ* describes pre-invasive neoplastic cell changes confined within either the ducts or lobules of the breast. Due to its *in situ* nature, there is no risk of metastatic behaviour. It is subclassified into ductal (DCIS) and lobular (LCIS) carcinoma-in-situ according to the site of the cell changes.

DCIS is a malignant, clonal proliferation of cells growing within the basement membrane-bound structures of the breast and with no evidence of invasion into surrounding stroma. It is graded histopathologically according to cell differentiation. The grade is related to the likelihood of progression to invasive carcinoma and the rapidity with which this is likely to occur.

In comparison, LCIS is not a premalignant lesion. It is an abnormal pathology which identifies those women at a higher risk of subsequently developing invasive breast cancer. In fact, the subsequent cancers that do occur are more likely to be of ductal origin.

2.3.2 Invasive Ductal Breast Cancer

Invasive ductal breast cancer (IDC) is the most common type of breast cancer and makes up 70 to 80% of cases. The malignant cancer cells penetrate the basement membrane of the ductal wall and invade the surrounding stroma. This allows potential for metastatic spread via the bloodstream or lymphatics.

A common clinical sign of IDC is a hard palpable breast mass. This results from a fibroblastic response to the invasion of tumour cells. Dimpling of the skin over the breast tissue, nipple inversion or retraction may also occur due to tumour infiltration of surrounding structures and traction on the suspensory ligaments.

Tumour cells can be identified histologically as they are much larger than normal epithelial cells. They can form a number of characteristic patterns within dense stroma. Grading of the tumour is determined by its differentiation from well differentiated tumours, with a typical glandular formation, to poorly differentiated tumours with solid sheets of pleomorphic cells.

2.3.3 Invasive Lobular Breast Cancer

Invasive lobular carcinoma (ILC) makes up 10% of breast cancers and is thus the second most common type found in the population. It is often found in breast tissue also containing IDC. It has a tendency to occur in both breasts as well as having a multicentric pattern.

Unlike IDC, clinical presentation is not always as obvious due to the variation of the stromal reaction to tumour invasion.

Histologically, its cells are in fact a similar size to normal epithelium and rather than form a variety of patterns, tumour cells either infiltrate the stroma as individual rows *(Indian file)* or form targetoid lesions. Very occasionally, the tumour might have features of both ductal and lobular carcinoma.

2.3.4 Other invasive breast carcinomas

Less common types of invasive breast cancer include medullary, mucinous, tubular and cribriform carcinoma.

Medullary carcinoma accounts for less than 5% of breast cancers. Similar to ILC, the stromal reaction might be minimal, making it difficult to diagnose clinically. Histologically there is evidence of haemorrhage and necrosis among the cells. The cells themselves have large nuclei of various shapes and appear in solid sheets which form a syncytium. Lymphocytes and plasma cells gather closely around these sheets.

Mucinous carcinoma makes up less than 5% of breast cancers also. Clinically it presents as a soft gelatinous mass. It can present on its own or in combination with other tumour types. The tumour is made up of isolated tumour cells (ITC) in pools of extracellular mucin as well as forming the occasional glandular structure.

Tubular carcinoma is found in less than 2% of breast carcinomas. Histologically it forms small pleomorphic gland randomly arranged. Cribriform carcinoma also is a rare form of breast cancer and is identifiable by its "sieve-like" pattern of growth. Both of these are again seen mixed with other tumour types or as individual cancers. The latter forms have a much lower chance of lymph node metastases (up to 10%).

2.3.5 Lymph node metastases

As explained earlier in this chapter, the axillary lymph nodes are the primary lymphatic filter for the breast and therefore the first to be involved in metastatic breast carcinoma. The "sentinel" lymph node, which is usually the largest lymph node in the axilla, is considered the first to receive the lymph drained from the breast and thus the most likely to harbor a metastasis. Most metastases appear to infiltrate the lymph node in the direction of lymphatic flow. Thus the first metastases would be found in the subcapsular sinus before penetrating towards deeper sinuses and finally invading the parenchyma.

The microscopic patterns of lymph node metastases tend to reflect the histological types of the primary breast tumour (Sharkey *et al* 1985). For example, in the case of IDC, the lymph

node metastases generally reproduce the nests and cords, as described above, with variable formation of duct-like spaces of the original tumour. (Figure 2.5)

Figure 2.5 **Metastatic ductal carcinoma with large aggregates of tumour cells plugging the lymph node sinuses (Haematoxylin, Phloxine and saffron stain) (Ioachim HL 2002)**

The cells themselves vary from cuboidal and monomorphic to large and highly pleomorphic with frequent mitoses. (Figure 2.6) Reaction to the invading carcinoma can cause enlarged follicles with reactive germinal centres, excessive histiocytosis, granuloma formation or desmoplasia. Thick bands of collagen might also form which can obliterate the entire parenchyma.

Figure 2.6 Metastatic ductal carcinoma forming rudimentary gland structures and highly pleomorphic tumour cells with large nuclear masses. (Haematoxylin, Phloxine and saffron stain) (Ioachim HL 2002)

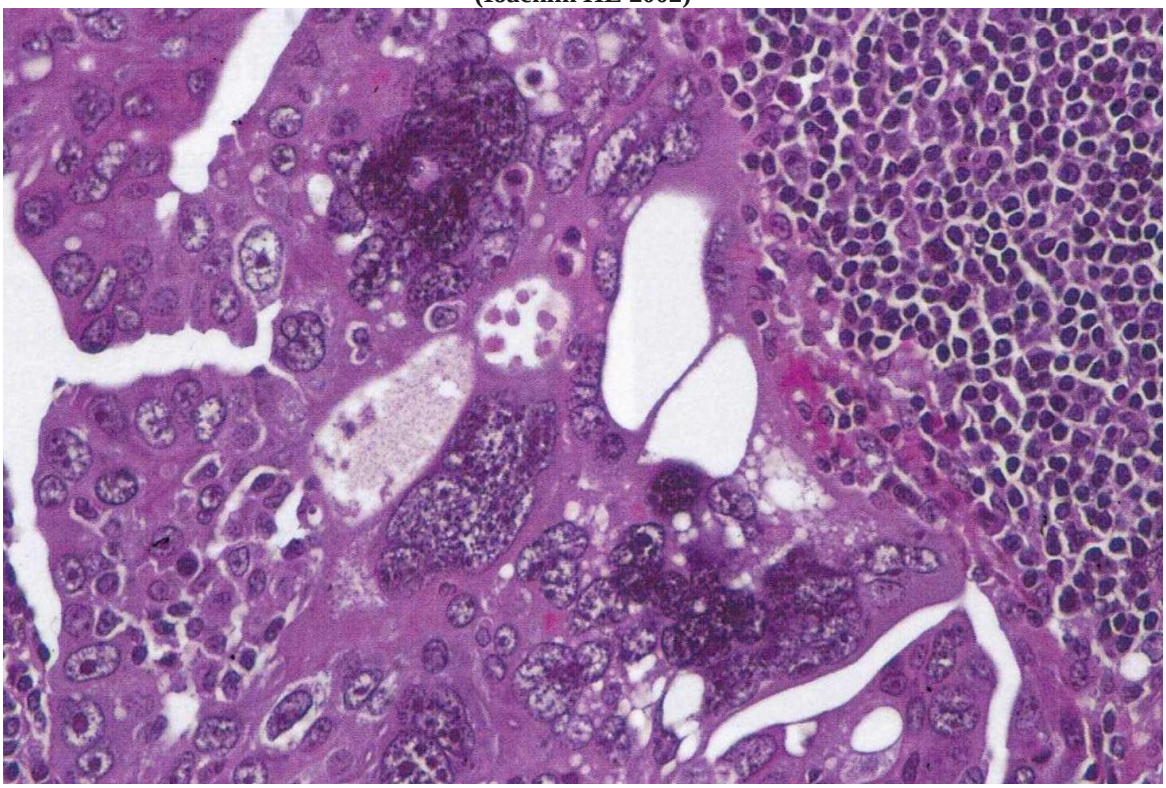

Recognition of lobular carcinoma metastases is not as straight forward. These metastases are distributed in the sinuses, sometimes deep down in the cortex or even the medulla without initial involvement of the marginal sinuses. When the metastases are recent, they only consist of single cells or tiny clusters which are difficult to identify and can be confused with histiocytes and endothelial cells (Figure 2.7). Focal signet ring differentiation is also common in lobular carcinoma metastases (Ioachim HL 2002).

Figure 2.7 Metastatic lobular carcinoma with single tumour cells surrounding an involuted lymphoid follicle. (Haematoxylin, Phloxine and saffron stain) (Ioachim HL 2002)

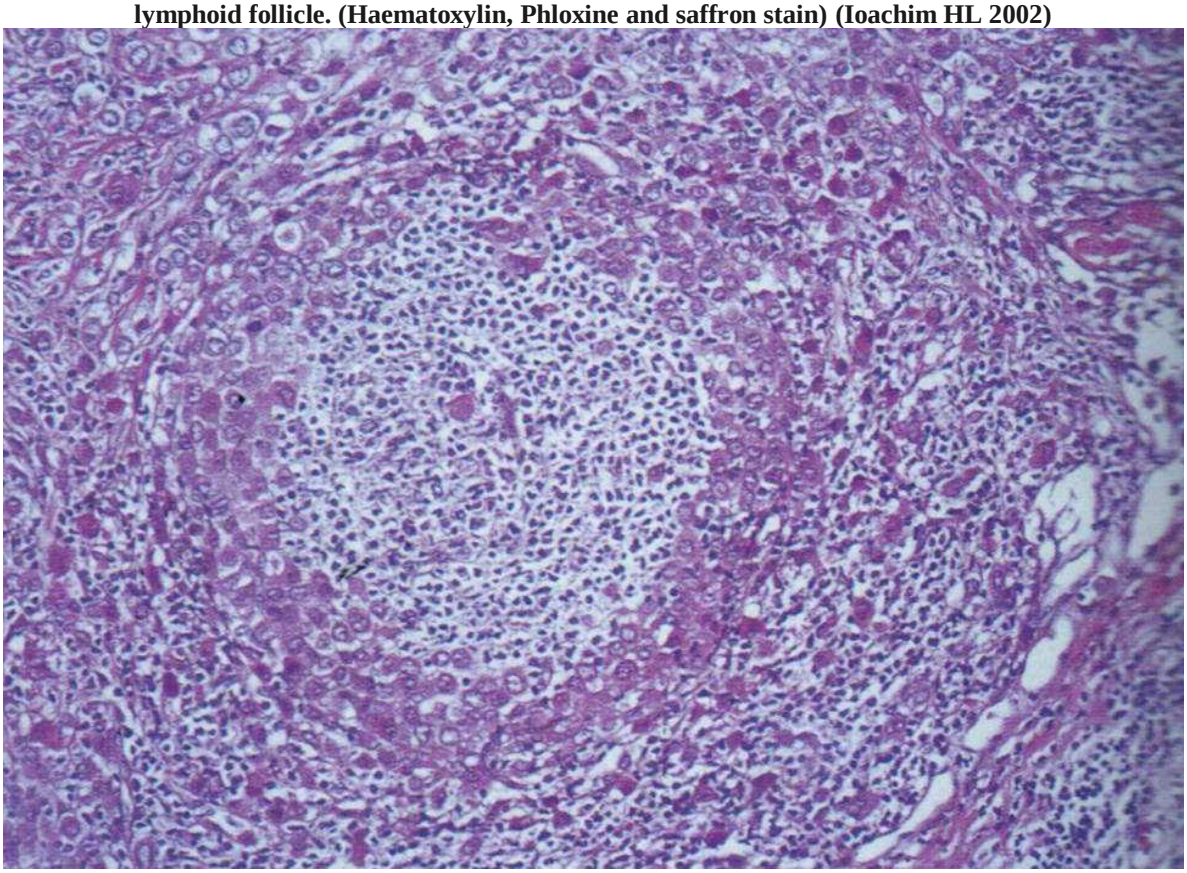

Histopathological analysis of lymph node metastases differentiates between micrometastases and macrometastases. The former describes a tumour deposit between 0.2mm and 2mm; the latter describes those deposits greater then 2mm in size. Those cells or clusters of cells less than 0.2mm in size are referred to as Isolated Tumour Cells (ITC).

2.3.6 Staging of breast cancer

The most popular means of staging breast cancer is the American Joint Committee on Cancer (AJCC) TNM classification system. This system describes the extent of cancer in the body. **T** describes the size of the tumour and invasion of surrounding tissue planes; **N**

describes regional lymph nodes that are found to be involved; **M** describes the presence of distant metastases.

The stage of a breast cancer can be based on clinical information (i.e. physical examination, biopsy and imaging) or, more accurately, on the pathological information following surgery. A summary of the TNM classification system for breast derived from the AJCC cancer staging manual (Edge SB 2010) is found in *Appendix A.*

2.3.7 Prognostic outcome

The Nottingham Prognostic Index was created in 1982 following a multiple-regression analysis of prognostic factors and survival in a series of 387 patients with primary breast cancer (Haybittle *et al* 1982). The score was based on lymph node stage, tumour size and pathological grade.

- **Lymph Node Stage**:
    - Negative lymph nodes have the most favourable prognosis.
    - Involvement of 4+ lymph nodes has the worst outcome.

- **Tumour Size:**
    - The most favourable prognosis is seen in those tumours < 2cm in size.

- **Grade**:
    - Grading is determined by the amount of nuclear pleomorphism, mitotic extent and the number of well formed tubules. Higher grades of differentiation have a least favourable outcome.

Histological type is also important in considering prognosis. IDC and ILC have the worst prognosis.

CHAPTER 3 VIBRATIONAL SPECTROSCOPY

3.1 Definition

Spectroscopy is the measure of the interaction between radiated energy and matter. Vibrational spectroscopy, which incorporates infra-red (IR) and Raman spectroscopy, is an analysis of the spectra produced by the vibrational modes of molecular bonds. It is therefore reflective of a molecule's structure and can thus be used to detect it.

Molecular vibrations can be excited via two physical mechanisms: the absorption of light quanta and the inelastic scattering of photons. Direct absorption of photons is achieved by irradiation of molecules with polychromatic light as in IR spectroscopy. Meanwhile, the scattering mechanism for exciting molecular vibrations requires monochromatic irradiation as seen in Raman spectroscopy. (Siebert *et al* 2008)

Whilst it is important to acknowledge the role of IR spectroscopy this study will concentrate on Raman spectroscopy.

3.2 Scattering of light

Usually, when light interacts with matter, it does not gain or lose energy. At a molecular level, a photon is essentially interacting with a substance molecule, causing polarisation of its electron cloud. This raises its *virtual* energy state before it returns to normal, releasing a photon. The energy released in this photon is the same as the incident photon. The wavelength therefore remains constant.

The photon released moves in any direction – it '*scatters*'. This complete process is called *Rayleigh scattering*.

Raman scattering, on the other hand, is an *inelastic* process whereby the light photons either lose or gain energy causing a change in wavelength. This is related to a molecule's *vibrational* modes determined by its bonds. (Figure 3.1)

If the molecule moves from a ground state to *virtual* state then back to a higher energy level (its *vibrational* state) the emitted photon has less energy – *Stokes Effect.*

If the molecule starts from a higher energy level or *vibrational* state when it is excited, then moves back to its ground state after reaching its virtual state, the photon emitted has gained energy – *Anti-Stokes Effect.*

Figure 3.1 Energy level diagram demonstrating the differences between Rayleigh and Raman scattering of light

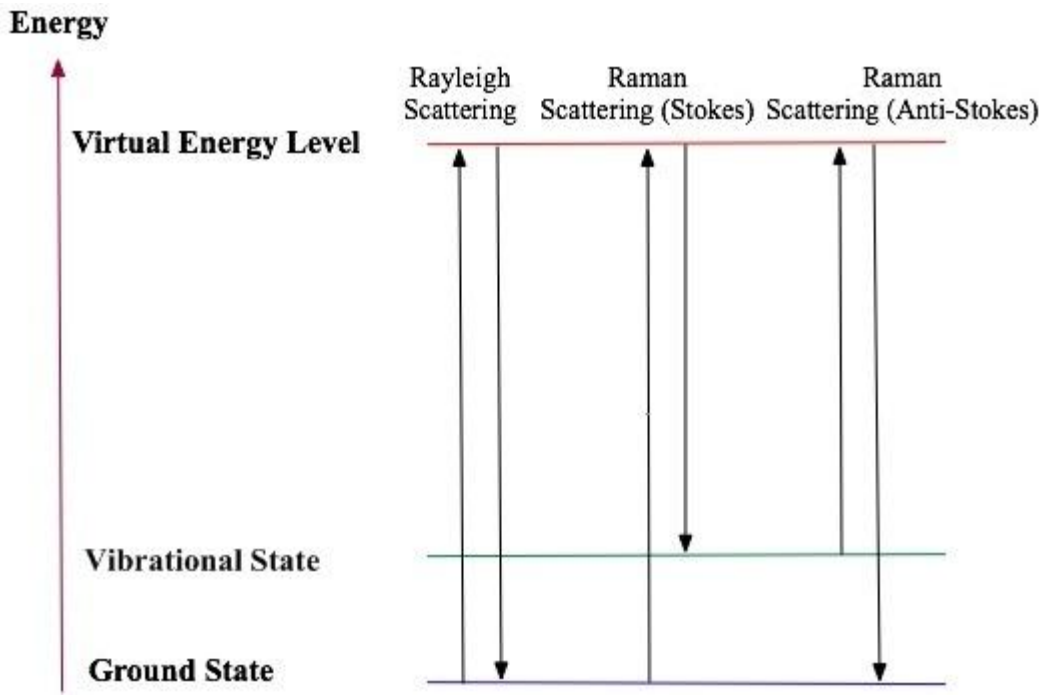

Only around 1 in 10^7 photons undergo Raman Stokes scattering whilst significantly less undergo Anti-Stokes. These photons are swamped by Rayleigh scattered photons. Modern spectrometers have therefore been designed and developed with filters that reject elastically scattered light.

3.3 Vibrational Modes

A molecule is an electrically charged neutral group of atoms held together as a single unit by electromagnetic forces resulting from the behaviour of their surrounding electron orbits. The vibrational mode of a molecule describes the relative positions of nuclei and electrons.

For a diatomic molecule, there is only one mode of vibration, the bond stretch. (Figure 3.2)

Figure 3.2 Bond stretch in a diatomic molecule

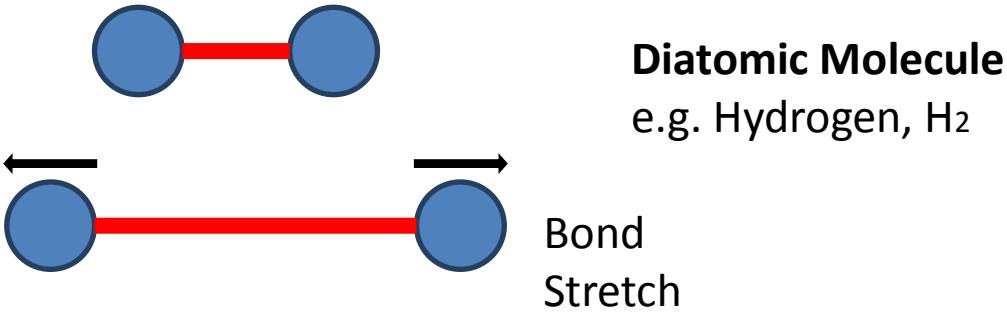

However, in molecules made up of more than two atoms, there are several modes of vibration owing to the various changes in bond lengths and angles (Figure 3.3).

Figure 3.3 Modes of vibration in a polyatomic molecule

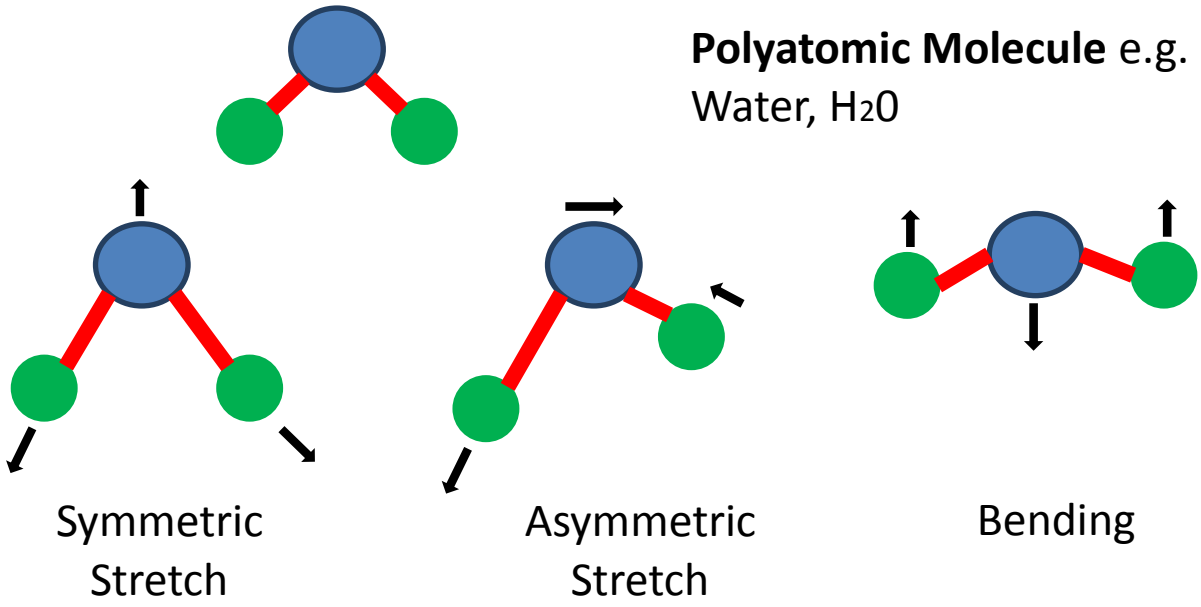

A *normal* mode for a specific molecule describes an independent, synchronous motion of atoms or groups of atoms that may be excited without leading to the excitation of any other *normal* mode and without involving rotation of the molecule (Atkins *et al* 2010).

The total number of *normal* vibrational modes of a linear polyatomic molecule can be calculated by the equation 3N-5 where N is the number of atoms within the molecule. For a non-linear polyatomic molecule, as shown in Figure 3.3, the equation is 3N-6.

Different vibrational modes have different energy values. Rotational modes also exist but do not contain as much energy as vibrational modes.

3.4 Raman Spectroscopy of vibrational modes

Raman spectroscopy is used to elucidate the energy changes produced by the transition between vibrational modes in the target molecule after illumination by incident light (*Raman Shift*). Analysis of the spectra can therefore help us to identify the specific bonds involved allowing us to determine the molecule's structural configuration.

However, for a molecule to be Raman active, the normal modes of vibration must be accompanied by a changing polarizability (Siebert *et al* 2008). Significant changes in polarizability are noted in electron-rich groups such as:

C=O C=N C=C

Those molecules containing these bonds will demonstrate intense peaks on their spectra. This enables recognition of particular molecules, e.g. collagen, lipid, actin, nucleic acid, protein, carbohydrate as a result of our pre-existing knowledge of their chemical structure.

Vibrational modes which leave polarizability unchanged are Raman inactive and therefore do not contribute to the Raman spectra.

3.5 Infra-Red Spectroscopy

Molecular vibrations can be also be excited by the absorption of light (Herzberg *et al* 1945) When infrared incident light is shone on a tissue, the molecules tend to absorb the photons. This also results in changes in the vibrational modes. However, the change results in an alteration in the *dipole moment* of the molecule. This gives the molecule the properties of two particles with opposite charges separated by a specific distance.

Certain molecules, such as water are more IR active than Raman active. Whilst the use of IR spectroscopy is therefore limited in vivo for this very reason, it can be used ex vivo to both validate and complement Raman.

3.6 Fluorescence

A common problem in studying Raman spectra is fluorescence. This occurs when the incident light, especially at the UV and visible end of the spectrum is absorbed by the tissue promoting an electron to an *excited* state, resulting in the dissipation of heat and the emission of a photon with a longer wavelength. To minimise this effect, Near-infrared (NIR) incident light with a longer wavelength is used as this is less easily absorbed, thereby minimising fluorescence.

CHAPTER 4 APPLICATION OF RAMAN SPECTROSCOPY

4.1 A Historical Overview

In 1923, Adolf Smekal, an Austrian physicist, first predicted the existence of inelastic scattering of light (Opel *et al* 2002). Five years later, in 1928, C.V Raman carried out a series of experiments in his Calcutta laboratories that demonstrated its existence (Raman *et al* 1928). He found that light scattered by a liquid, such as benzene, contains sidebands in pairs symmetrically disposed around the frequency of incident light. The shifts were identical to the frequencies of some of the IR vibrational spectral lines of the liquid. Landsberg and Mandelstam observed similar effects in solids such as quartz (Opel *et al* 2002). The concept was named the *Raman effect* and earned Raman himself a Nobel Prize in 1930.

In the next 75 years, Raman spectroscopy became an important tool for studying elementary excitations in gases, liquids and solids. However, progress was initially slow due to the limited sources of radiation and technology for detection and analysis of the spectra.

With the introduction of the working laser in 1960 (Maiman *et al* 1960) the charged coupling device in 1970 (Boyle *et al* 1970) and the development and application of Fourier

Transform techniques to present the detected photon energy as spectra (McClure *et al* 1988), studies into the use of Raman spectroscopy were renewed with increased enthusiasm.

4.2 Application of Raman Spectroscopy

In the past few years, the extent of progress in instrumentation for Raman spectroscopy has improved such that robust, high quality data is now possible. The main developments are noted to be:

- *In vivo probes* for biopsy targeting;
- Histopathology tools;
- Deep Raman tools for *in vivo* analysis in solid organs;
- Enhancing signal production.

These significant milestones are described in detail by Kendall (Kendall *et al* 2009). Initially, work was focussed on differentiating normal tissue and advanced cancers. However, with developing technology and complex analytical methods, we have been able to move towards the diagnosis of neoplastic change at much earlier stages.

4.2.1 Technique of tissue Raman Spectroscopy

The technique of Raman Spectroscopy involves the illumination of a tissue sample with monochromatic radiation usually at a near-infrared wavelength. The inelastically scattered photons are then measured, thereby probing the vibrational and rotational modes of the molecules within the sample.

Whilst Raman had to use sunlight focused through a telescope to acquire sufficient intensity for the scattered signal, modern spectrometers use lasers at a single wavelength along with more sensitive detectors to obtain better results. CCDs have also been incorporated to enable the measurement of a whole spectrum at once.

Furthermore, the main difficulty in Raman spectroscopy has been found to be the prevention of overlap of the Raman signal by stray light from Rayleigh scattering. Interference notch filters are frequently employed, which filter out wavelengths within approximately 100 cm^{-1} of the laser wavelength. Holographic diffraction gratings might also be incorporated which result in much less stray light than ruled gratings (University of Cambridge 2007). Figure 4.1 demonstrates a simplified diagram of a Raman Spectrometer's operation.

Figure 4.1 Simplified Raman Spectrometer (University of Cambridge 2007)

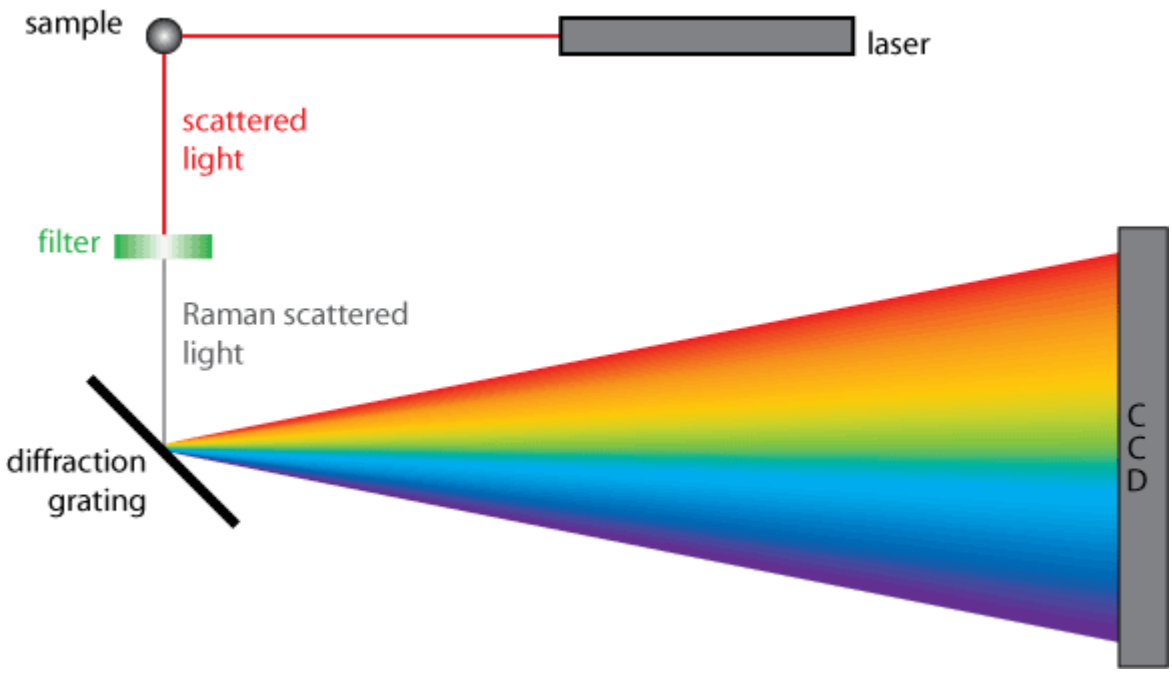

The subsequent spectrum produced is a plot of the inelastically scattered photon intensity as a function of the energy difference between the incident and scattered light *(Raman Shift).*

Figure 4.2 is an example of Raman shift demonstrated by axillary lymph node spectra which are positive for metastases compared with negative lymph nodes (Horsnell *et al* 2010).

Figure 4.2 Mean normalised spectra of metastatic nodes versus non-metastatic nodes (Horsnell *et al* 2010)

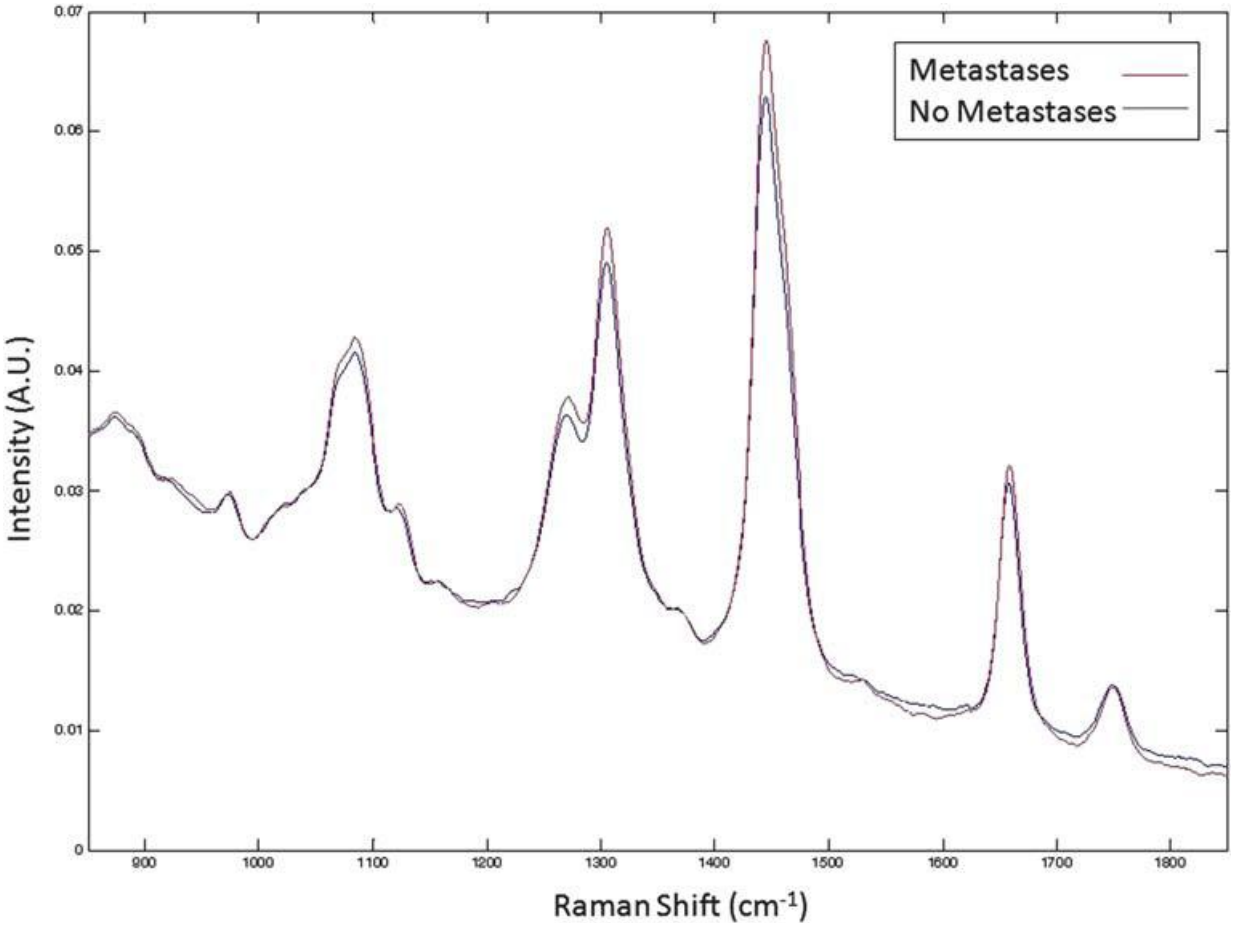

The intensity of individual peaks is proportional to the concentration of the molecular constituent giving rise to that peak. A database of peak positions and assignments has been created from several studies in order to aid in detection of various molecules. (Kendall *et al* 2002).

Multivariate data analysis methods might be used with Raman Spectroscopy to help classify tissue samples based on their biochemical makeup. Principal component analysis (PCA) is an unsupervised data reduction technique which describes the major sources of independent variation in the data. The data is fed into a supervised classification system such as linear discriminant analysis (LDA) using factual information about the samples, such as histopathological analysis. These techniques of spectral analysis will be described later on in Chapter 5.

4.2.2 Raman spectroscopy probes

Fibre optic probe technology has offered the opportunity to both illuminate and collect Raman spectra *in vivo*. However initial studies showed that fibres can generate Raman signals themselves, as demonstrated by Shim (Shim *et al* 1999). Elastically scattered light returning along the collection fibres themselves may also create further background signal.

Thus probe designs had to be able to prevent these interference signals. For example, holographic and metal oxide edge filters have been investigated for their ability to reject Rayleigh scattered light. (Kendall *et al* 2009). More recently, *in vivo* probes coupled to a spectrometer have been introduced as a means of real-time measurement and analysis. It is this design on which this research is based.

The majority of work in this research group has looked at the use of *in vivo* assessment of oesophageal tissue to identify the subtle pre-malignant changes related to carcinogenesis (Kendall *et al* 2011). Raman probes offered non-invasive optical biopsy with the benefit of reduced number of random normal biopsies being collected and processed. Furthermore, it could assess resection margins of tissue intra-operatively. This would reduce the need for further repeat procedures which are currently required when histological assessment, performed days later, demonstrates inadequate resection.

Other areas of research have included the use of probes for *in vivo* assessment of the cervix (Liu *et al* 2011), head and neck (Harris *et al* 2010), colon (Molckovsky *et al* 2003) and bladder (Crow *et al* 2005). The use of probes for assessing breast disease and lymph nodes will be further discussed later on in this chapter.

4.3 Clinical need for Raman spectroscopy

Cancer diagnostics plays a pivotal role both as an important tool for early detection and through its role in cancer management.

Early detection of cancer has been shown to improve the chances of successful treatment and decrease mortality rates (UK Trial of Early Detection of Breast Cancer Group. 1999) Ongoing research has demonstrated that many cancers develop through pre-malignant stages. Eradication of these abnormal cells prior to systemic invasion will prevent

development of the cancer further. This type of disease prevention not only benefits the patient but also healthcare providers, particularly in a climate where finances are limited. The clinical need for techniques that can identify or detect these pre-malignant biochemical changes is thus considerable.

It should be noted, however, that the danger of this technology is overtreatment. It is therefore important to have a clear understanding of progression and the natural history of the disease in question.

Diagnostics as part of cancer management is equally important. A quick, non-destructive, efficient and cheap tool that is as non-invasive as possible is required.

Currently, histopathology is the "gold standard" for most cancer diagnostics. However, this method is invasive, requiring removal of tissue biopsies often randomly and unnecessarily. Tissue fixation, sectioning and staining follow which can be expensive and time-consuming. Analysis is very much subjective and is often associated with inter-observer disagreement (Montgomery *et al* 2001).

Recent advances in Raman spectroscopy have promoted it to a level at which it might be seen as a comparable diagnostic tool. *Ex vivo* studies have demonstrated its potential in

aiding the histopathologists in the identification and classification of subtle biochemical changes related to carcinogenesis rather than complete dependence on morphology. Raman spectroscopy can provide rapid, high resolution, non-destructive data which is not influenced by the subjectivity of histopathology. Spectral classification models are currently under development (Shetty *et al* 2006) which are trying to understand biochemical changes using a variety of multivariate techniques such as Principal Component Analysis leading to Linear Discriminant Analysis. PCA is non-supervised which explores the variance in data. LDA correlates these changes with the gold standard of histopathology (Horsnell *et al* 2010). The decision is therefore not itself based on the subjectivenes of morphology, making it advantageous. There are other multivariate techniques also such as Partial Least Squares Discriminant Analysis which can demonstrate causes of discrimination, using loadings and weights, thus giving it a unique role in exploratory data analysis.

In vivo, Raman spectroscopy offers the potential for "optical biopsy" with important clinical benefits. Excisional tissue biopsy carries risks of bleeding and perforation of a viscus as well as removal of normal tissue unnecessarily. *In vivo* Raman spectroscopy would obviate the need for this, thus reducing trauma to the patient, reducing the clinician workload, and reducing secondary repeat procedures. It would also decrease the rate of re-excisions of areas of dysplasia or malignancy by accurately defining resection margins (Hanlon *et al* 2000).

4.4.1 Raman spectroscopy in breast disease

Raman Spectroscopy has the potential to impact breast cancer diagnostics in a number of ways including the *in vivo* detection and identification of abnormal lesions as well as by means of a histopathological classification tool which may provide a measure of prognostic biochemical changes.

Fourier Transform Raman was first used to discriminate breast cancer tissue in 1991 (Alfano *et al* 1991). More recent studies, using 830 nm excitation and dispersion spectrometers, showed discrimination of normal, benign and malignant breast tissue (Shafer-Peltier *et al* 2002), (Manoharan *et al* 1998). Raman mapping of breast duct epithelia identified different cellular compounds using PCA and k-means clustering (Kneipp *et al* 2003) such as cytoplasm and nuclei.

Calcifications detected by mammography during national screening programmes can be an indicator of a malignant breast lesion. However, mammography alone does not reliably classify calcifications as benign or malignant. In fact, only up to 25% of these lesions are found to be malignant on core biopsy (Haka *et al* 2005). Raman spectroscopy has been shown to distinguish between the different chemical make-up of benign and malignant calcifications (Haka *et al* 2002). It has also highlighted the potential to probe deep breast calcifications *in vivo* by means of Kerr-gated spectroscopy (Baker *et al* 2007). Although this form of technology is not necessarily appropriate *in vivo* due to safety and practicality, other deep Raman techniques have stemmed from it as a result at the Rutherford Appleton

Laboratory, UK. Spatially offset Raman spectroscopy (SORS) has demonstrated discrimination between different calcification types at 8.7 mm depth. This finding has lead to the possibility of detecting lower calcification concentrations as well as those at greater depths (Stone *et al* 2007). Transmission Raman spectroscopy has enabled signal recovery and identification of calcifications at depths of 27 mm and at calcification volume densities within physiological levels (Stone *et al* 2008).

Recently, studies on mammary tumours in mice have correctly identified all normal and mastitis Raman spectra and 91% of tumour spectra (Kast *et al* 2008). Normal tissue surrounding the tumour, given the term "tumour bed", was interrogated as a separate data group. Suspicious atypical cells were discovered and were found to be different from normal, tumour, and mastitis tissue, proposing a pre-neoplastic process as might be expected. A further study demonstrated 99% of non-tumour tissue and 95% of tumours induced in mice were correctly classified by Raman spectroscopy (Thakur *et al* 2007).

A Raman study to diagnose benign and malignant lesions in human breast tissue differentiated between invasive carcinoma, fibrocystic change, fibroadenoma, and normal tissue (Haka *et al* 2005). The diagnostic algorithm used in the study yielded a sensitivity of 94%, specificity of 96% and an overall accuracy of 86% for distinguishing cancerous tissue from normal and benign. Raman spectroscopy has also differentiated between the nuclear grades (low, intermediate and high) of ductal carcinoma in situ (DCIS) and invasive ductal carcinoma (IDC) of the breast (Rehman *et al* 2007). This group observed spectral change in the intensity of fatty acid chains, phospholipids, cholesterol, proteins and nucleic acids with

increasing nuclear grade. It was concluded that high-grade carcinoma tissue is rich in acylglyceride while low-grade carcinoma tissue is rich in protein.

More recent work has included surface enhanced spatially offset Raman spectroscopy. Stone (Stone *et al* 2011) recovered for the first time multiplexed surface enhanced Raman scattering (SERS) signals noninvasively from a depth of 20 mm in tissues and reconstructed these to produce a false colour image. A secondary finding was also that Raman signals from SERS nanoparticles could be recovered non-invasively from samples of the order of 45–50 mm thick. This was huge step forward in the ability to detect and identify vibrational fingerprints within tissue and offered the opportunity to adapt these particles and this approach into a clinical setting for disease diagnosis.

4.5 Raman Spectroscopy and lymph nodes

The use of Raman in the assessment of lymph nodes in breast cancer has hitherto been limited, the majority of work being done on the breast itself and other tissues. Assessment of Silicone lymphadenopathy appears to be the starting point for its use in analysing lymph nodes. In 1993, Frank used Raman spectroscopy to examine lymph node biopsy specimens from women with ruptured breast implants containing silicone gel (Frank *et al* 1993). Since silicone has a strong Raman peak, the lymph nodes containing silicone inclusions were clearly identified.

The first paper to demonstrate Raman mapping of malignant spread in axillary lymph nodes was published in 2003 (Smith *et al* 2003). Tissue was collected after surgical resection for breast cancer. A portion of one lymph node from each case was removed and snap frozen. The samples were later cut for spectroscopy and for histological assessment, using a microtome. Spectra were collected from the lymph node tissue and analysed using Principal Component Analysis (PCA).

The spectral maps were compared with white light images of the same section and the stained histological slides of parallel sections. The intensity of the principal component spectra could thereby be examined for specific lymph node features described by the histologist. Additionally, the relative presence of molecules identified in PCA, such as lipids, could be assessed in various areas of nodal section.

The authors emphasized that the long running time required for spectroscopic analysis of this nature meant that this detailed mapping was not suitable for real-time clinical use itself. However, it was an ideal way to map features common to lymph nodes so that a diagnostic model could be created for comparison and prediction of pathology of new samples. Further spectra would be required.

Two years later, a classification model using 59 lymph node sections from breast cancer patients demonstrated 91% sensitivity and 93% specificity for correct classification of cancerous node spectra (Smith *et al* 2005).

In 2008, Isabelle (Isabelle *et al* 2008) took lymph node samples removed during oesophagectomies for primary cancer. The lymph nodes were cut in half; one half was sent for histological analysis; the other half was snap frozen and later underwent both Raman and IR spectroscopic analysis. Out of 20 lymph nodes, 11 were malignant and 9 benign. The authors demonstrated the biochemical differences between the mean pathological spectra of these two groups. Benign lymph nodes had increased lipid and carbohydrate concentrations and lower nucleic acid concentrations. The latter is assumed to be due to greater mitotic activity in the malignant nodes. The results of the study showed a training performance for Raman and IR spectroscopy of >94% for the differentiation between benign and malignant tissue. It was however a small study and so further supporting data would be needed to strengthen their results. It was also noted that most spectral peaks had contributions from more than one biochemical component and so assignment of the peaks to specific biochemical changes was often speculative.

4.5.1 Raman spectroscopy probe in the intra-operative assessment of lymph nodes

Horsnell (Horsnell *et al* 2010) demonstrated *in vitro* results of the use of a Raman spectroscopy probe to evaluate the status of axillary nodes sampled from patients with newly diagnosed breast cancer. 38 axillary nodes were sampled from 20 patients. Half a node was sent to histology whilst the other half was snap frozen and later assessed in the laboratory with the hand-held Raman probe. Histological assessment demonstrated 25 nodes to be negative and 13 nodes to be positive. The mean spectra demonstrated evident

differences between positive and negative nodes. Principal Component Analysis was employed to demonstrate these differences further. The results of the PCA were then used to perform linear discriminant analysis which had been trained by the histopathology results. The training model achieved a remarkable 97% sensitivity and 99% specificity at differentiating the two groups.

Internal validation of these results demonstrated a sensitivity for the method of up to 92% and specificity of up to 100% in differentiating normal and metastatic nodes.

Horsnell (Horsnell, 2012), has explored the use of the probe in the theatre setting. Lymph node samples were collected from 50 patients undergoing axillary surgery for breast cancer. After resection, the nodes were bisected. Each half was assessed using a portable Raman spectroscopy device with a mean assessment time of 138sec. The node was then sent for post-operative histopathological assessment as is usual for current breast operations.

Of the 209 lymph node halves, histology classified 181 as negative and 28 as positive. 1507 spectra were obtained from the negative nodes and 300 from the positive nodes. Principal component analysis followed by linear discriminant analysis showed a specificity of 99% and a sensitivity of 92% at differentiating between the two groups. However the strength of these figures might be questioned given the imbalance in data between the positive and

negative groups. Significant differences in the peaks associated with fatty-acids were also noted.

CHAPTER 5 MATERIALS AND METHODOLOGY

5.1 Ethical approval

Ethical approval for the project was granted by Gloucestershire Local Ethics Committee. Those patients eligible for participation within the study had a diagnosis of breast cancer and were due to undergo axillary lymph node surgery as part of their disease management.

All patients were consented pre-operatively either in a pre-admission outpatient clinic or on the ward. The risks and benefits were explained to the patient and an information leaflet supplied. Only those patients who signed the consent form were included in the study.

5.2 Tissue collection

Collection of the lymph nodes for intraoperative analysis took place in main theatres at Cheltenham General Hospital.

Those patients undergoing sentinel lymph node biopsy have radioactive technetium isotope injected around the ipsilateral nipple pre-operatively in the radiology department. Lymphoscintigraphy images are taken and triangulated body marking is used to mark

where the sentinel lymph node(s) are. Once anaesthetised in theatre, Patent Blue V dye is also injected around the nipple.

Following a small axillary incision and careful dissection of the axilla by either the consultant surgeon or specialist registrar, the sentinel lymph node(s) is detected with assistance from the lymphoscintography images, triangulated skin markings, blue dye and handheld gamma probe. The lymph node(s) are excised using sharp dissection with or without the use of diathermy.

Those patients undergoing axillary lymph node clearance do not undergo any pre-operative procedures. An incision is made in the axillary skin and the whole axilla is carefully dissected in order to remove all lymph nodes in the anatomical space. 2 or 3 lymph nodes are taken at random from the dissected tissue for spectral collection.

Once removed from the body, the lymph nodes are handed over and taken through to the side room away from the operating theatre. Using a scalpel, any fatty tissue is excised before the node(s) are carefully bisected. Each half is labelled ‘a’ or ‘b’ and numbered according to the order in which they are excised as well as the gamma probe reading.

For example, the first sentinel node is labelled 1a and 1b once bisected; the second sentinel node is labelled 2a and 2b, and so on.

Following collection of spectra, as described below, the lymph node halves are placed into separate pots of formalin, carefully marked with the patient's details, date and lymph node number and sent to the histology department, as per protocol.

5.3 Histopathology

Within the histology laboratory, the specimens are examined macroscopically before being processed in cassettes and then put into hot paraffin wax to protect the tissue. Once cooled the wax blocks are cut into very thin slices, using a microtome, which are then put onto glass slides and undergo H+E and immunohistochemistry staining for microscopic analysis. Reporting of the histopathology results is validated by a consultant histopathologist.

The classification used for the lymph nodes is as follows:

0 Negative lymph node in an axilla with no positive lymph nodes

1 Negative lymph node in an axilla containing positive lymph nodes

2 Isolated Tumour cells

3 Lymph nodes with micrometastases only

4 Lymph nodes with macrometastases

5 Fat only (no lymphatic tissue)

The timing and accuracy of tissue collection and histopathological analysis are not affected by the intra-operative Raman studies in any way. No tissue loss or damage occurs and, similarly, no extra tissue is required for the studies. The overall management of the patient's disease is not altered which is paramount in delivering patient care.

5.4 Tissue Samples

Tissue samples were collected between July 2011 and February 2012, with 37 patients taking part in the study. 27 patients underwent sentinel lymph node biopsy whilst the remaining patients underwent axillary clearance.

The primary breast carcinoma for 31 patients was invasive ductal carcinoma and for 2 patients was invasive lobular carcinoma. Of the remaining 4, there was 1 medullary carcinoma, 1 papillary carcinoma, 1 tubular carcinoma and 1 sarcoidosis.

5.5 Raman spectroscopy

Measurements of Raman spectra from the lymph nodes collected took place in a side room in main theatres. In order to comply with laser safety standards, local rules were adhered to:

- Controlled area and designation of access to the room
    - No windows

- Locked door
- Appropriate signs on the door

- Protective eyewear for all those in the room
- Authorised users only gaining access to room
- Adverse Incident procedure in place

5.5.1 Raman instrumentation and set-up

The $B_{\&}WTEK_{INC}$ MiniRam II Portable Raman Spectrometer was used to measure spectra from each lymph node half (Figure 5.1).

Figure 5.1 $B_{\&}WTEK_{INC}$ MiniRam II Portable Raman Spectrometer

The spectrometer contains a Class 3B diode laser, $\lambda = 785nm$, invisible near infrared beam with a maximum power output of 350mW and 174mW accessible beam from the probe. The laser beam is transmitted down a fibre optic delivery system attached to a probe head fitted with a shutter.

The spectrometer is connected to a laptop computer with the appropriate BWSpec^{TM} software installed for data collection as well as control of laser excitation.

The set-up of equipment is based on that created by Horsnell in his recent doctorate lymph node studies at Cranfield University, which are, as yet, unpublished and awaiting formal assessment. The handheld probe is mounted on a metal clamp stand with the probe facing upwards so that the lymph node half can sit on top during measurement of spectra. The probe head itself is mounted with a light impermeable case (Figure 5.2). During excitation of the laser and spectral collection, a black impermeable sheet is secured over the top of the case to prevent any light from entering.

Figure 5.2 Set-up of the portable Raman Spectrometer

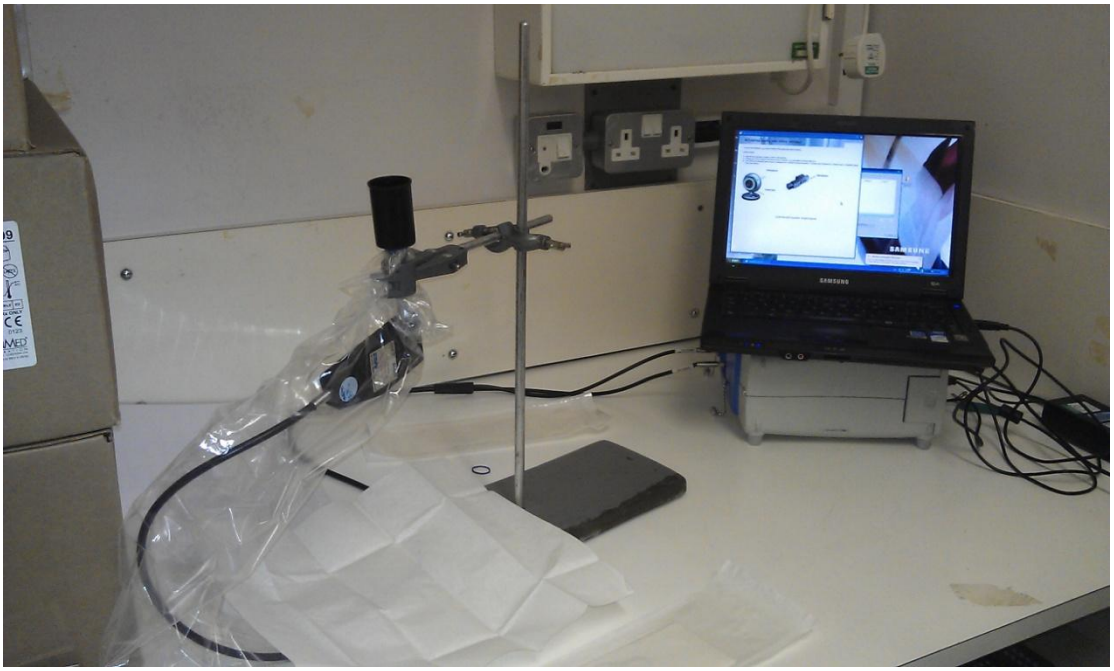

For each patient, a protective disposable sterile probe sheath is used to cover the probe in order to prevent cross-contamination between samples as well as to keep the equipment clean.

5.5.2 Calibration

In order to detect fluctuations over time within the spectrometer, spectral measurements are performed at the start of every theatre list for Blue Patent V Dye, PTFE, cyclohexane, green glass and a plastic pipette tip. The results are calibrated into the end results for the lymph nodes during analysis (see Chapter 6).

5.5.3 Measurement of lymph node spectra

Following bisection of the lymph nodes into halves as detailed above, each half is placed on the probe tip and the impermeable case covered with the black sheet. Spectra are measured for 16 x 1 sec acquisitions and the average presented graphically. 5 sets of mean spectra are taken per lymph node half. As a variation to Horsnell's model the lymph node half is in fact moved at random between each set so that spectra are taken from 5 areas of the lymph node half. 30 seconds between the 16sec acquisitions was given to allow manual manipulation of the lymph node.

The rationale behind the above variation is attributed to work done by Smith (Smith 2005) who looked at probe models which were designed to mimic the use of a probe on a cut lymph node surface. Three models were constructed comparing results from the selection of 5, 10 and 20 points on tissue sections.

Figure 5.3 Diagram showing approximate selection pattern for probe models (Smith 2005)

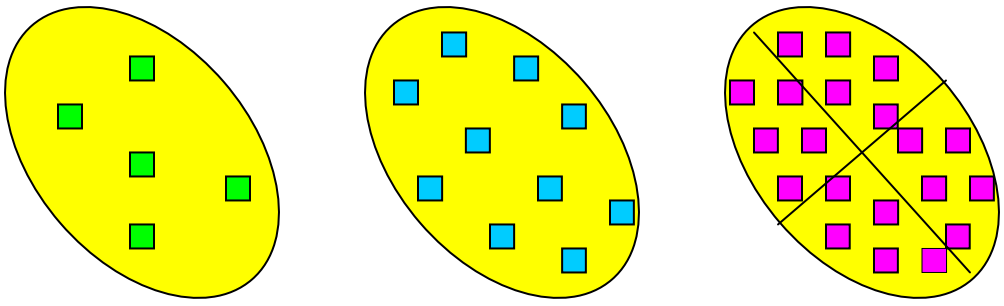

Analysis of results demonstrated that the highest percentage of correctly classified positive spectra was achieved in the Probe 20 model (86%). The highest percentage of correctly classified negative spectra was achieved in the Probe 10 model (93%), only 3 % higher than the Probe 20 model. In general Smith's models demonstrated that results for sensitivity and specificity were optimised when a greater number of sample blocks were collected from each node section.

Movement of the lymph node does indeed increase the time taken for data collection by an extra 2 minutes per lymph node half. However, in the clinical setting this is negligible. Furthermore a more sophisticated probe design might incorporate this movement so that this time is reduced.

5.6 Spectral Analysis

Following data processing, multivariate statistical analysis is employed in order to identify and quantify differences between spectra. Peak assignments are incorporated in order to identify biochemical assignments for spectral peaks.

5.6.1 MATLAB

Initially, for each lymph node half, spectral and histological data is entered into MATLAB which is a software programme for algorithm development, data analysis, visualization, and numerical computation.

During data processing, prior to analysis, the software was used to clean the data. Spectra with an average value greater than 25000 was removed as the CCD saturates at this level giving a poor signal. Data with a value less than 2000 produced insufficient signal to noise ratio to make a clear decision. This latter figure is arbitrary but arrived at from experience.

Graphs demonstrating Raman shift against intensity were subsequently created giving a qualitative visual demonstration of peak differences between the histological groups.

5.6.2 Peak assignments

The identification of spectral peaks with regards to their specific biochemical properties is carried out using previously published data. It should be noted that significant overlap can exist between peaks making identification complex. In this study, I have used peak assignments from Kendall (Kendall *et al* 2002). The details of these will be discussed further in chapter 6 with the results.

5.6.3 Principal Component Analysis (PCA)

PCA is a variable reduction procedure which extracts relevant information from large complex data sets. It is incorporated as a data analysis technique where measurements are obtained on a number of observed variables in order to develop a smaller number of artificial variables, Principal Components (PCs). The components are produced in order of variance so that the first component (PC1) represents the greatest degree of variance over the set, followed by PC2, and so on.

By applying PCA to the spectral dataset, each spectrum is allocated a score for each principal component which indicates the representation of each component within that spectrum. It follows that the sum of each PC multiplied by its score should recreate the original spectrum. Examination of each PC allows the identification of biochemical features which differ maximally through incorporation of peak assignments.

ANOVA was applied to the PCs in order to identify the most significant.

5.6.4 Linear Discriminant Analysis (LDA)

LDA is a supervised multivariate analytical technique which is applied to the Principal Components. It is a form of data analysis which further maximises separation between groups and minimises variation within groups. The PC scores are used as input giving an output of Linear Discriminant score values.

5.6.5 Cross validation

To assess the significance of the results a “leave one out” cross validation test was performed due to the small dataset. From this, sensitivity, specificity and overall performance could be determined.

CHAPTER 6 RESULTS AND DISCUSSION

Data collection took place in the main theatres at Cheltenham General Hospital between July 2011 and February 2012.

A total of 37 patients were included in the study, all of which were undergoing either axillary lymph node clearance or sentinel lymph node biopsy as part of the management for breast cancer.

The number of lymph nodes sampled per patient varied between 1 and 3, giving an average of 1.65 and mode of 1 per patient.

6.1 Histopathology

122 lymph node halves were collected in total. Table 6.1 demonstrates the histopathological findings of the lymph node halves where a positive lymph node contains evidence of metastases and a negative lymph node does not.

Six lymph nodes were found to have different histopathological findings in each of their halves. Table 6.2 demonstrates the histological variation of these lymph nodes.

Table 6.1 Histology of lymph node halves

HISTOPATHOLOGICAL FINDINGS	NO. LYMPH NODE HALVES
Total Negative Lymph Node Halves	**87**
Negative in an axilla containing positive lymph nodes	25
Negative lymph node in an axilla with no positive lymph nodes	62
Total Positive Lymph Node Halves	**30**
Lymph nodes with micrometastases only	2
Lymph nodes with macrometastases	28
Fat only (no lymphatic tissue)	**4**
Isolated Tumour cells	**1**
TOTAL	**122**

Table 6.2 Histological variation within lymph nodes

Lymph node half	Histopathological findings
1a	Fat only (no lymphatic tissue)
1b	Negative
2a	Fat only
2b	Negative
3a	Isolated Tumour Cells
3b	Negative
4a	Micrometastases
4b	Negative
5a	Macrometastases
5b	Negative
6a	Micrometastases
6b	Macrometastases

6.2 Raman Spectra

5 spectra were measured for each lymph node half giving a total of 610 spectra.

The spectral data was entered into MATLAB® software for comparison with the histopathological findings and subsequent analysis.

Figure 6.1 demonstrates the spectra from all data collected excluding those spectra which have been rejected. The latter includes spectra with either an average value of greater than 25000, suggesting fluorescence, or less than 2000, suggesting insufficient signal. The spectra have been background subtracted with a third order polynomial and normalized by adjusting the total area under the curve to equal 1.

Figure 6.2 shows the mean spectra of all the above results with polynomial background subtraction, normalisation and smoothing. The values of the significant Raman peaks are annotated and correspond to specific bonds within the molecules. Table 6.3 demonstrates the possible bonds responsible for these peaks (Kendall *et al* 2002).

Table 6.3 Raman Peak assignments (Kendall 2002)

Raman Shift Value (cm^{-1})	Nearest quoted value in literature (cm^{-1})	Assigned Bond	Tissue/substance	Author
873	873	hydroxyproline (C-C)	Collagen	Nie (1990)
967	966	Hydroxyapatite	Calcified plaque	Clarke (1987)
		Desmosine/isodesmosine	Elastin	Manoharan (1996)
		Triple helix vibrations	Collagen type I, skin dermis	Fendel (1988)
1072	1072	P-O asymmetric stretch	Chicken leg bone	Nie (1990)
	1074	Triglycerides	Adipose - aorta	Baraga (1992)
1084	1084	Lactic acid	DL-Lactic acid ($C_3H_6O_3$)CH_3-CHOH-COOH	Pilotto (2001)
	1085	Phenylalanine(amino acid)	Protein	Hartman (1973)
1130	1130	Lipid	Human skin	Carter (1998)
		Trans C-C stretch-phospholipids	Human brain tissue, glioma grade III	Mizuno (1994)
1180	1180	Tyrosine	Breast	Manoharan (1998)
1271	1271	Amide III	Collagen	Mahadevan-Jansen (1998)

1305	1304 1306	CH_3CH_2 twisting Lipid	Oleic acid methyl ester Human colon	Frank (1995) Redd (1993)
1369	1365 1372	Guanine, tryptophan Lipid	 Human colon	Hartman (1973) Redd (1993)
1446	1445 1447	CH_3CH_2 deformation in collagen CH_2 bending mode CH_3CH_2 bending modes in bovine albumin	Sigma Aldrich C7774 Normal breast tissue Sigma Aldrich A2153	Kendall (2002) Manoharan (1998) Kendall (2002)
1535	1529 1540	Carotenoid Amide II	Normal colon Bovine Insulin	Redd (1993) Sajid (1997)
1660	1660-1670	Amide I (C=O stretch)	Unordered protein secondary structure	Carey (1982)
1750	1750	C=O	Skin dermis	Fendel(1988)

Intensity changes and peak shifts at these points may therefore highlight significant differences between histological tissue types thus allowing identification.

Figure 6.3 separates the spectra into the different histological classifications. There is a visible difference in peak ratio at 1072:1084 for negative nodes compared with nodes containing macrometastases. This represents a possible change in triglyceride to lactic acid balance, the positive nodes containing a greater proportion of triglycerides compared to

lactic acid. Furthermore, the peak ratio at 1072:1130 is less for positive nodes than negative nodes, suggesting a smaller triglyceride to phospholipid ratio. Looking at micrometastases compared to macrometastases, the collagen to lipid ratio (1271:1305) is much less for those nodes with micrometastases.

Figure 6.4 demonstrates the average spectra collected from lymph node halves reported as histologically positive in comparison to those reported as histologically negative. The differences mentioned above are re-emphasised. Also of note is the difference in peak ratio at 1369:1446, the negative nodes demonstrating a higher proportion of collagen in comparison to lipid content. The peak shape at 1535, possibly corresponding to amide II or carotenoid, is also visibly different between the two histological groups, suggesting a greater concentration in positive nodes.

Figure 6.5 elicits the spectral difference between these two groups. The most intense differences are again reiterated as above. Intensities greater than zero correspond to benign nodes whilst those below zero correspond to malignant nodes.

The overlap between peak shapes for the average and standard deviations of both negative and positive lymph node halves are manifested in Figure 6.6. Comparing the two figures,

there is certainly some visible overlap between the two groups and this will be discussed later on in the chapter when considering linear discriminant analysis of the data.

Within the positive lymph node halves, 2 out of 30 were found to have micrometastases rather than macrometastases. A difference between the spectra from these two classifications is shown in Figure 6.7. For the macrometastases, greater peak intensities are seen at 1072 (triglyceride concentration), 1130 (lipid concentration) and 1446 (collagen concentration). The peak ratio 1271:1305 (collagen: lipid) is again demonstrated and is much less for those nodes with micrometastases. Another difference is the peak shape at 1180 which represents tyrosine. However, as will be discussed later, with only 2 lymph node halves showing micrometastases, the strength of these comparisons are very weak. Worthy of note though is the similarity in peak shapes and ratios of the micrometastases to benign nodes. This could be a reflection of a higher proportion of normal tissue being present and malignant changes not being picked up. More specimens with micrometastases would need to be analysed in the future before any conclusion can be made.

Within those lymph node halves reported as negative, 25 out of 87 were sampled from an axilla also containing positive lymph nodes. Figure 6.8 demonstrates that there is visually very little difference between the spectra for these nodes in comparison with those sampled from a negative axilla.

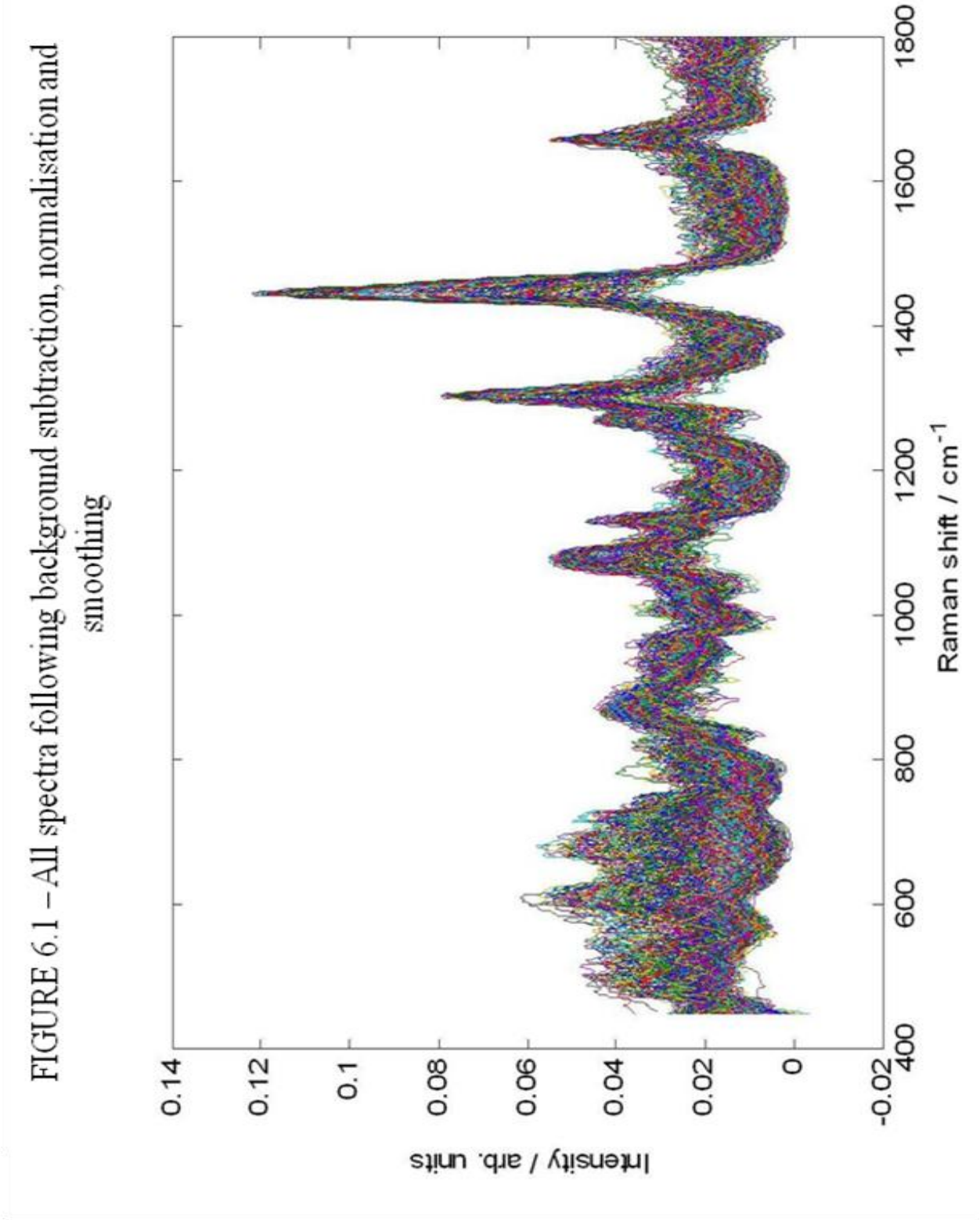

FIGURE 6.1 – All spectra following background subtraction, normalisation and smoothing

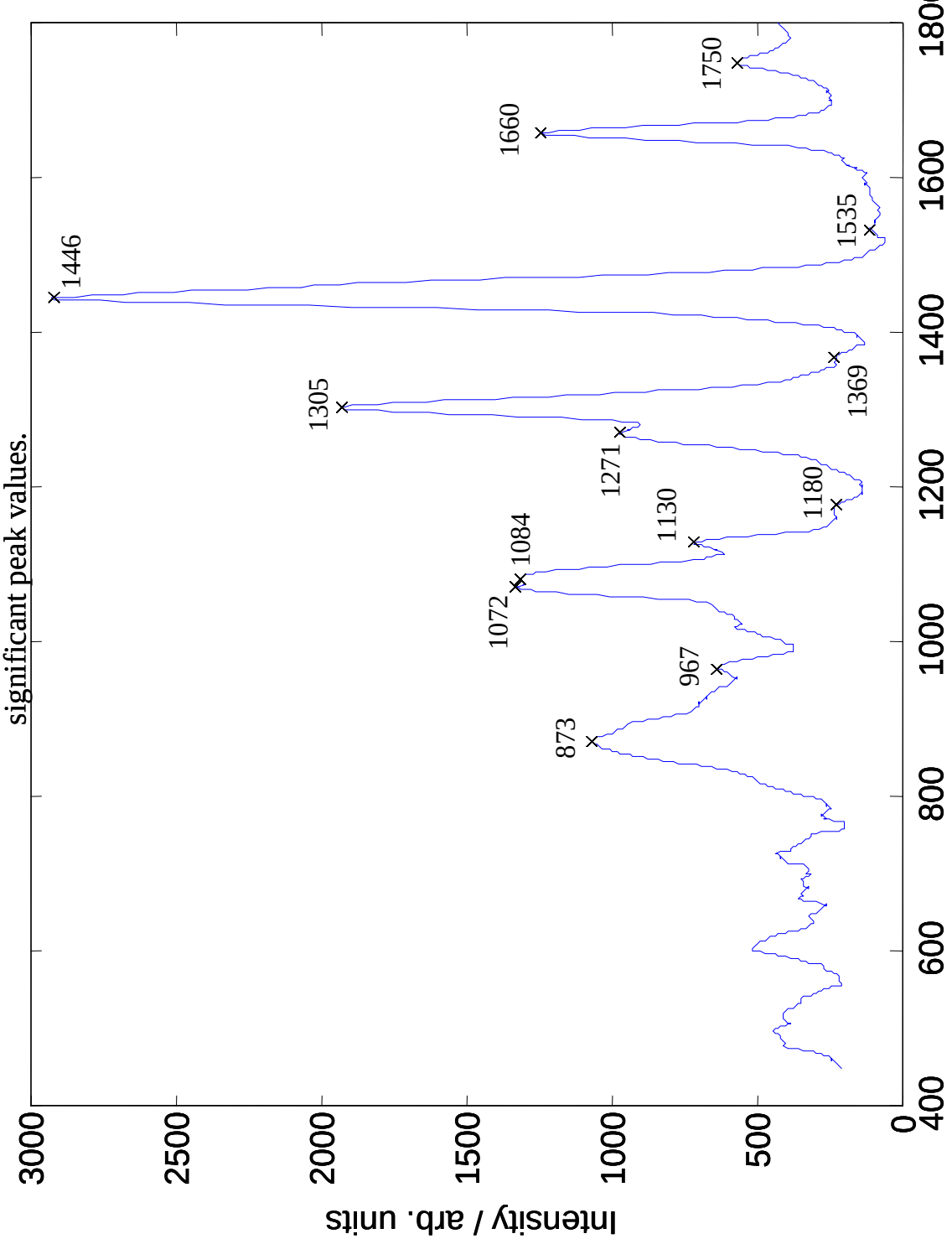

FIGURE 6.2 – Mean of all data (with polynomial background subtraction) including annotation of significant peak values.

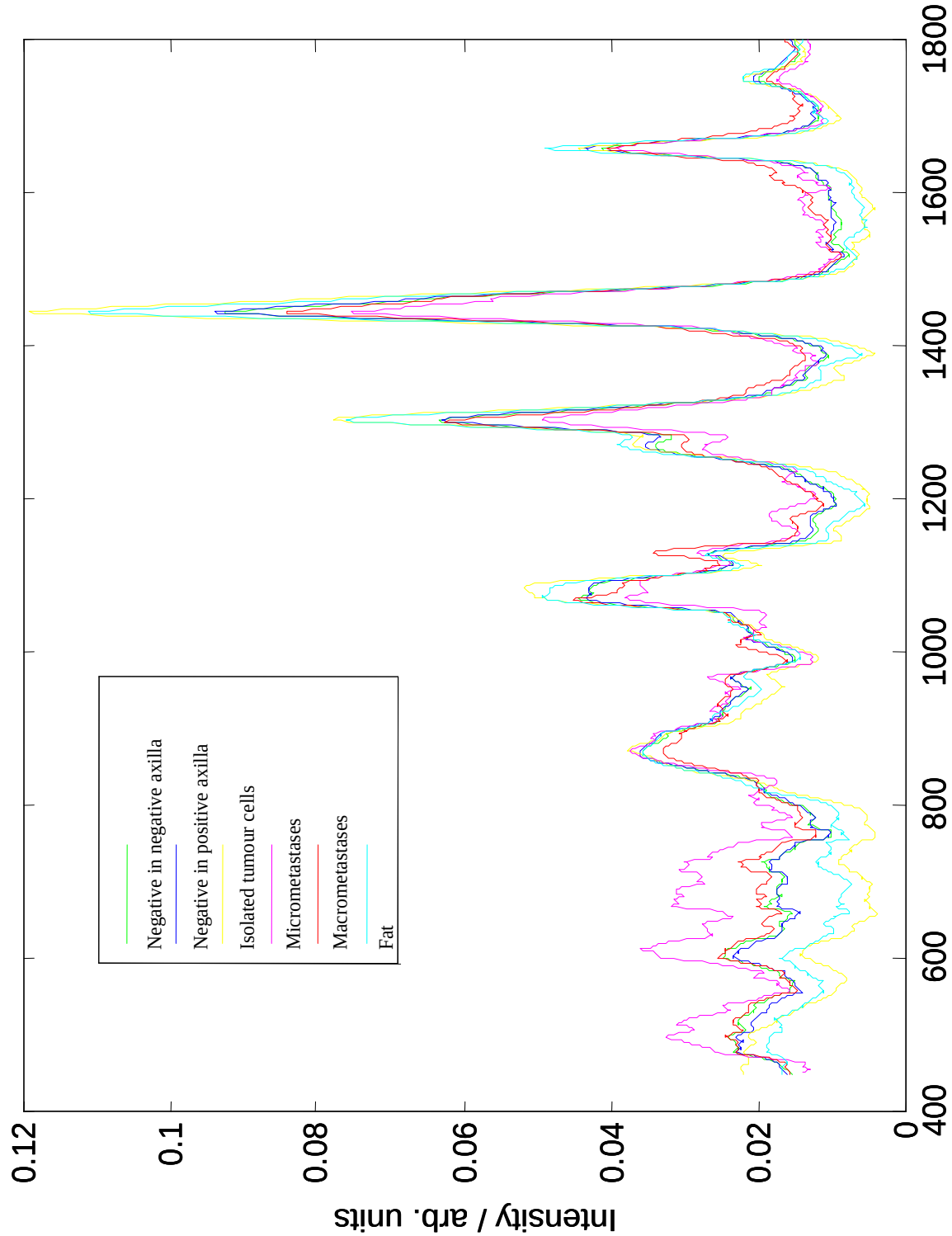

FIGURE 6.3 – Spectra of different histopathological classifications

FIGURE 6.4 – Spectra of positive lymph node halves in comparison with negative lymph node halves

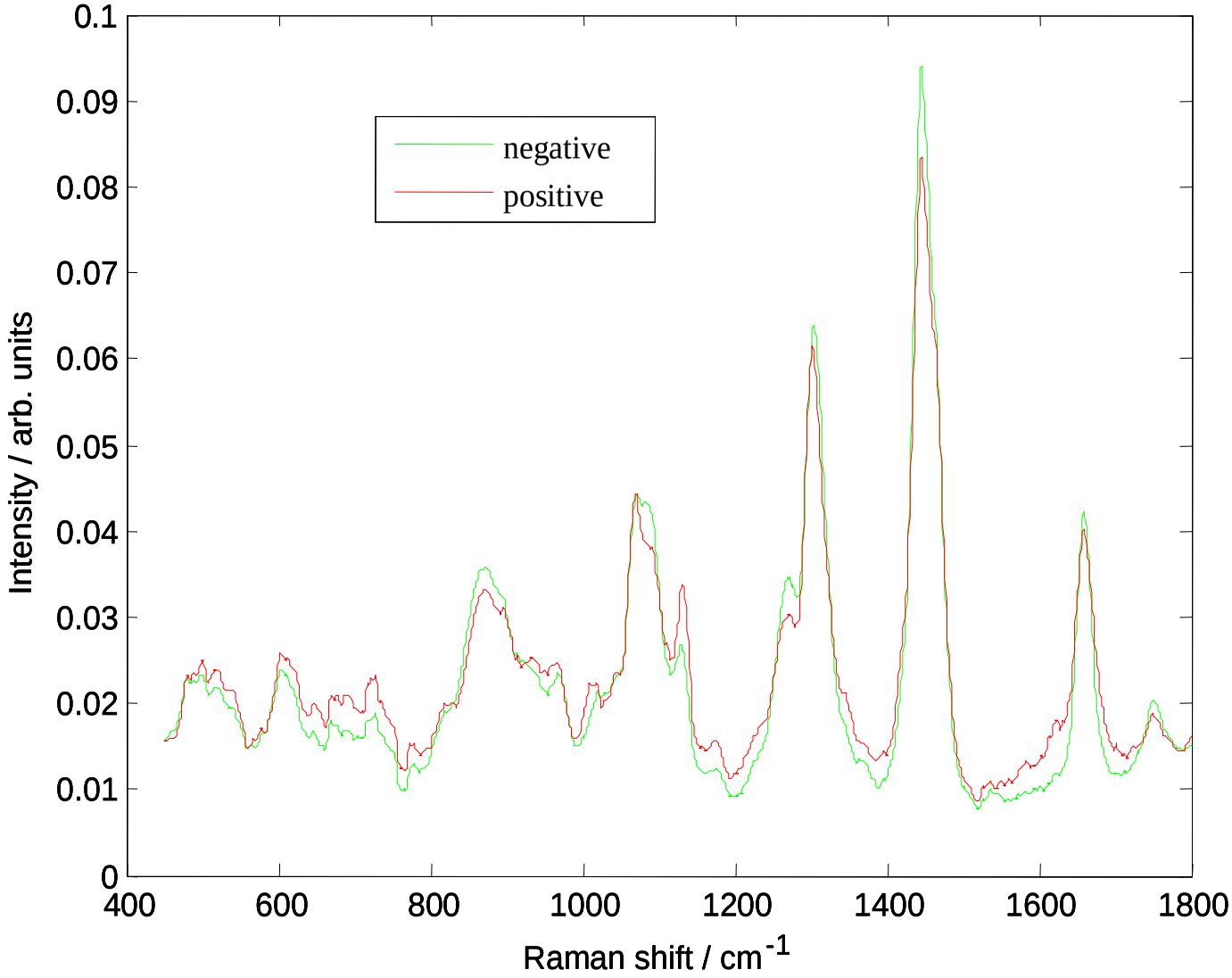

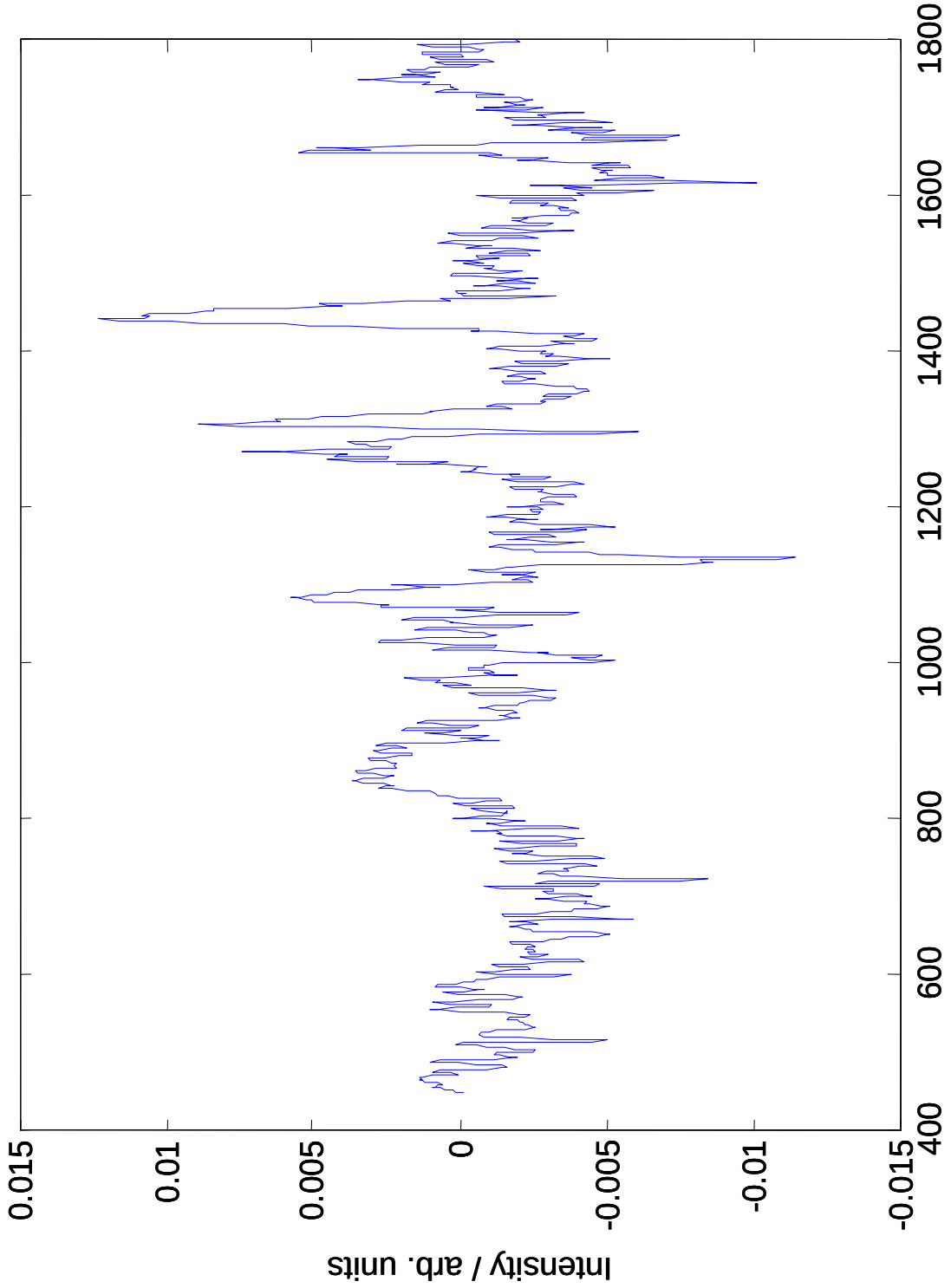

FIGURE 6.5 – Spectral difference between positive and negative lymph node halves

FIGURE 6.6 – Mean and standard deviation values for the positive and negative lymph node halves

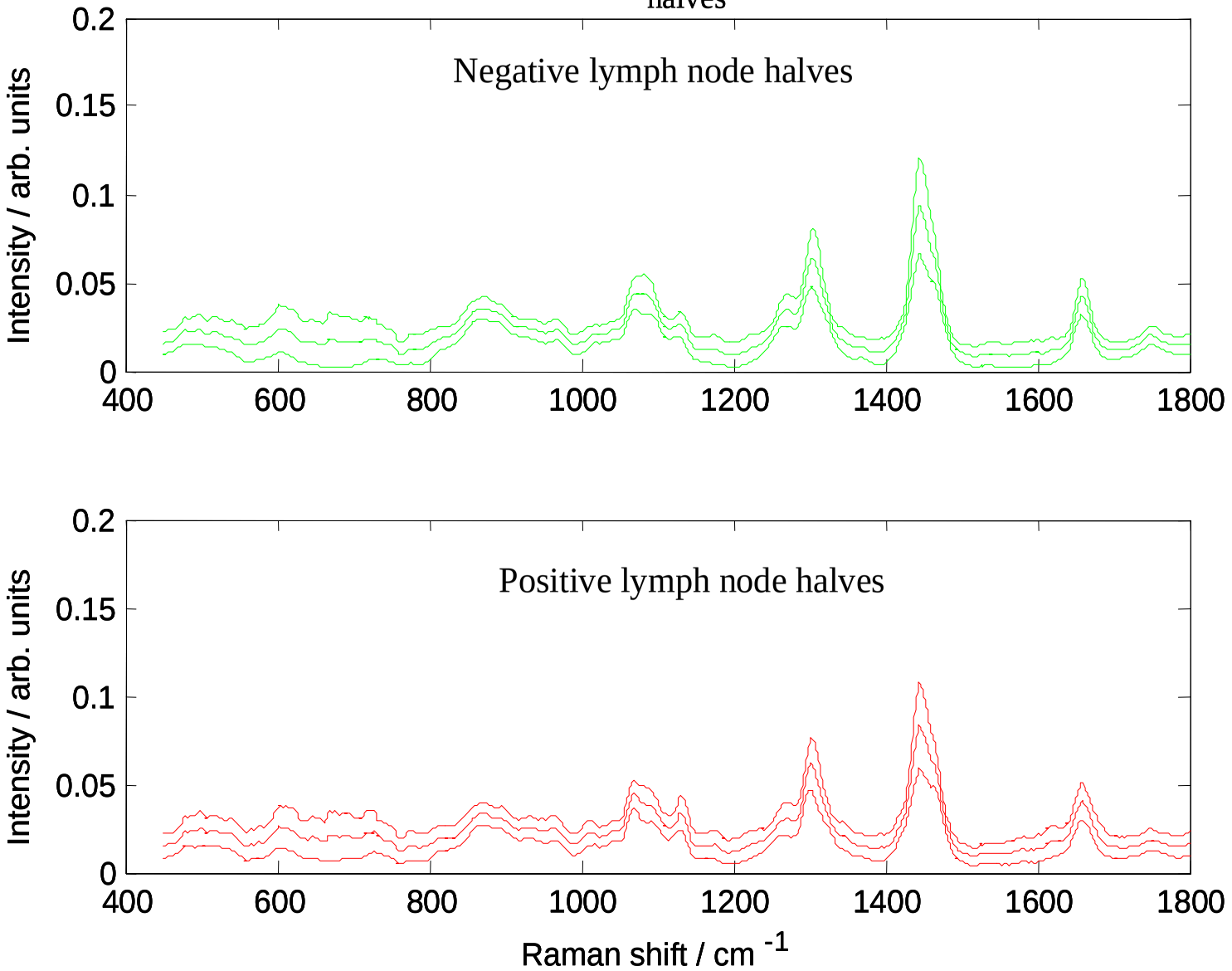

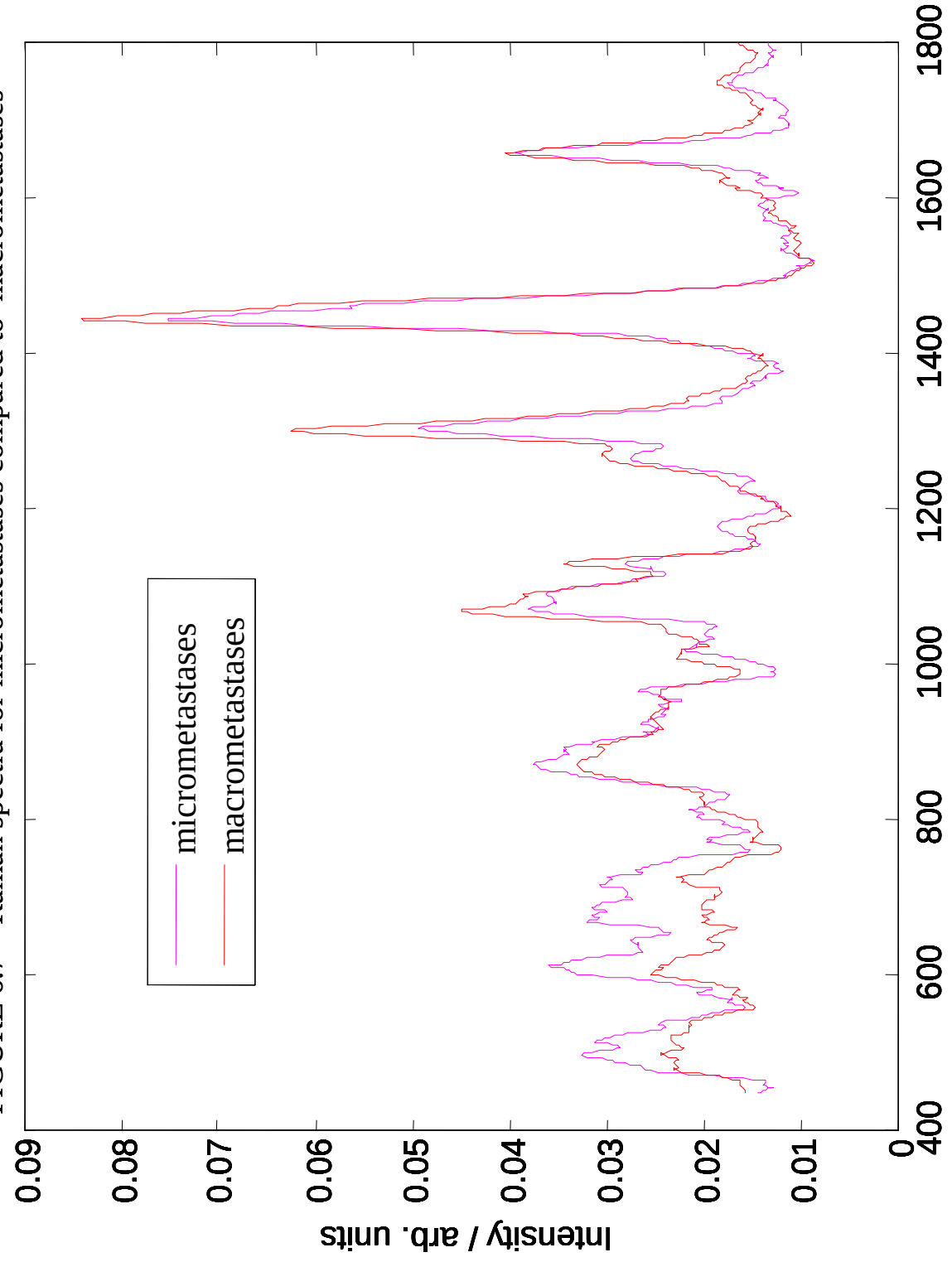

FIGURE 6.7 – Raman spectra for micrometastases compared to macrometastases

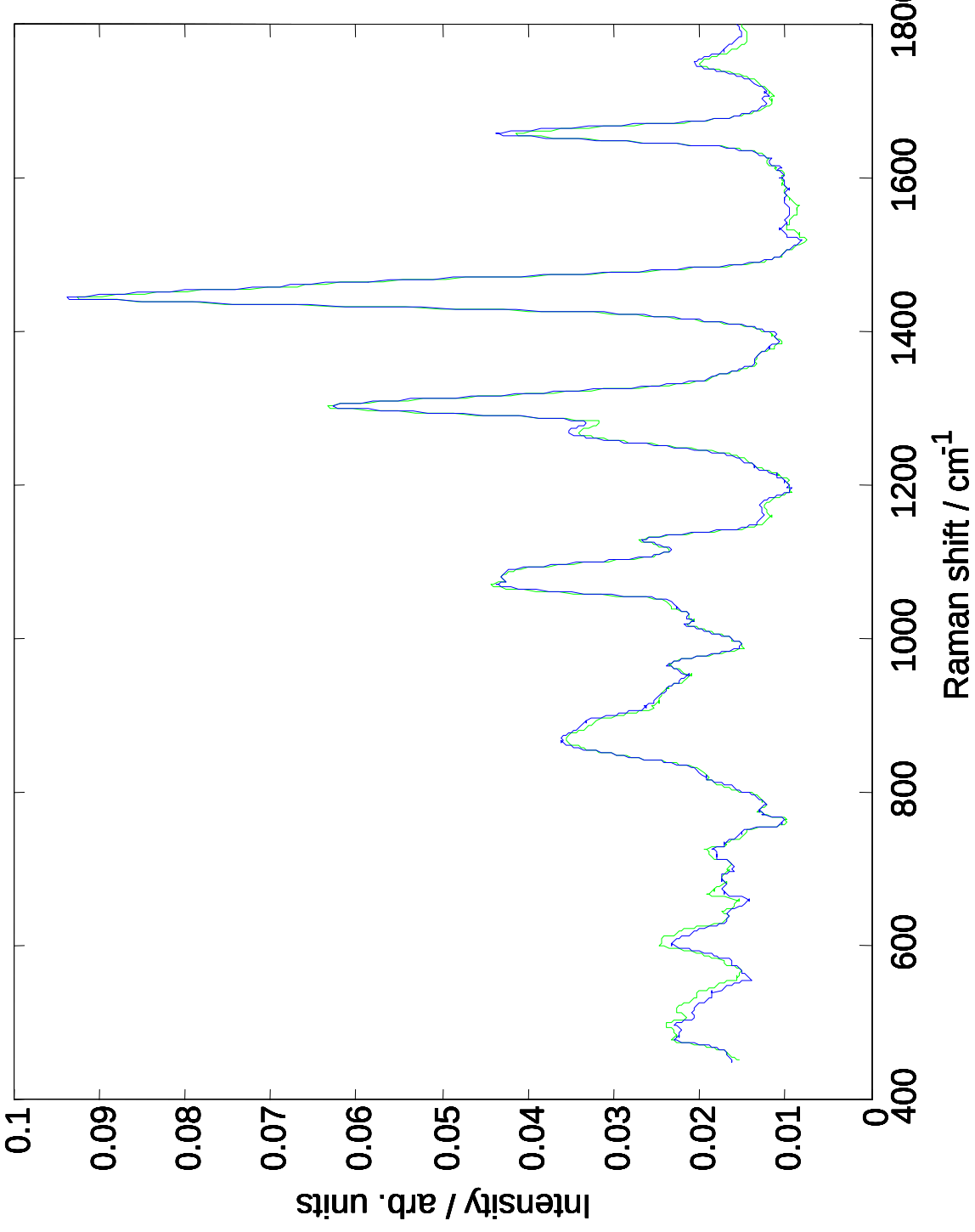

FIGURE 6.8 – Spectra for negative nodes in a positive axilla (green) compared to negative nodes in a negative axilla (blue)

6.3 Analysis of results

The data collected was used to produce various training models. Cross validation via a "leave one node out" scenario was used to produce an overall training performance figure for both a "6 group" model and "2 group" model.

Principal component analysis was performed for each model to demonstrate the most significant spectral peak changes between the histopathological groups.

ANOVA of the principal components demonstrate the components with the most significance. A scatter plot of these thus demonstrates the degree of separation, as described later on in this chapter.

Application of Linear Discriminant Analysis, through further data reduction, was able to demonstrate the degree of separation between groups and variation within groups. An example of PCA-fed LDA is demonstrated by Kendall in determining whether Raman Spectroscopy can be used to detect dysplastic cells with a higher probability of progression to cancer in the oesophagus. (Kendall *et al* 2011)

6.3.1 The "6 Group" Model

This model demonstrated the likelihood of correctly predicting in which of the 6 histopathology groups the node would be found.

In order to further reduce any errors caused by any possible changes to the instrument over time, the data was recalibrated using a green glass fluorescent standard. Although normalisation and smoothing still took place, there was no background subtraction on the data used in the multivariate analysis described above as it would add in more error.

Figure 6.9 demonstrates the "mean centred spectral data". This is created through subtraction of the mean spectra from the overall data set shown in Figure 6.1. It therefore shows the variation in spectral peaks between data.

The principal components (PCs) for this dataset are demonstrated in Figure 6.10. The order of PCs demonstrates the areas of largest spectral variation.

Application of ANOVA to the PCs highlights the peak changes shown in PC 6 and 7 as the most significant.

PC6 highlights peak changes at 1072, 1084, 1272, 1305 and 1446. Using the peak assignments from Table 6.3, the data would suggest changes in concentration for triglycerides, phenylalanine, amide III, lipid and collagen between the histological groups. PC7 further describes changes in amide II (1535) and amide I (1660) concentration.

The reasons behind these varying concentrations are not necessarily clear but various research papers can provide support for this finding. Liu (Liu *et al*, 2012) measured the fasting serum lipid profile of 324 breast cancer patients with and without synchronous distant metastases. The results of his study demonstrated that hyperlipidaemia is significantly associated with distant metastases in breast cancer patients. Similarly, Mbaye (Mbaye *et al*, 2012) showed a 79.3% increase in the rate of phenylalanine in cancerous tissues in women with breast cancer.

Proliferation of tumour cells can certainly account for variation in protein concentrations and amides. Furthermore, collagen, a major component of connective tissue, supports the structure of breast tissue and can also signal to cells. Normally, collagen is a seemingly unorganized mass of curvy threads. However, a recent study has found that collagen looks different at various stages of breast cancer which may account for variation in concentration demonstrated here (Conklin *et al*, 2011).

The scatter plot in Figure 6.11 further demonstrates the separation of these six groups. Whilst there is considerable overlap between histological types, there is an element of separation visible between the benign and malignant histology types.

The macrometastases have high levels of PC7 which appears to discriminate the positive nodes from the negatives. However, the negative nodes in a positive axilla also had increased levels of PC7. PC6 though discriminated the macrometastases from these negative nodes.

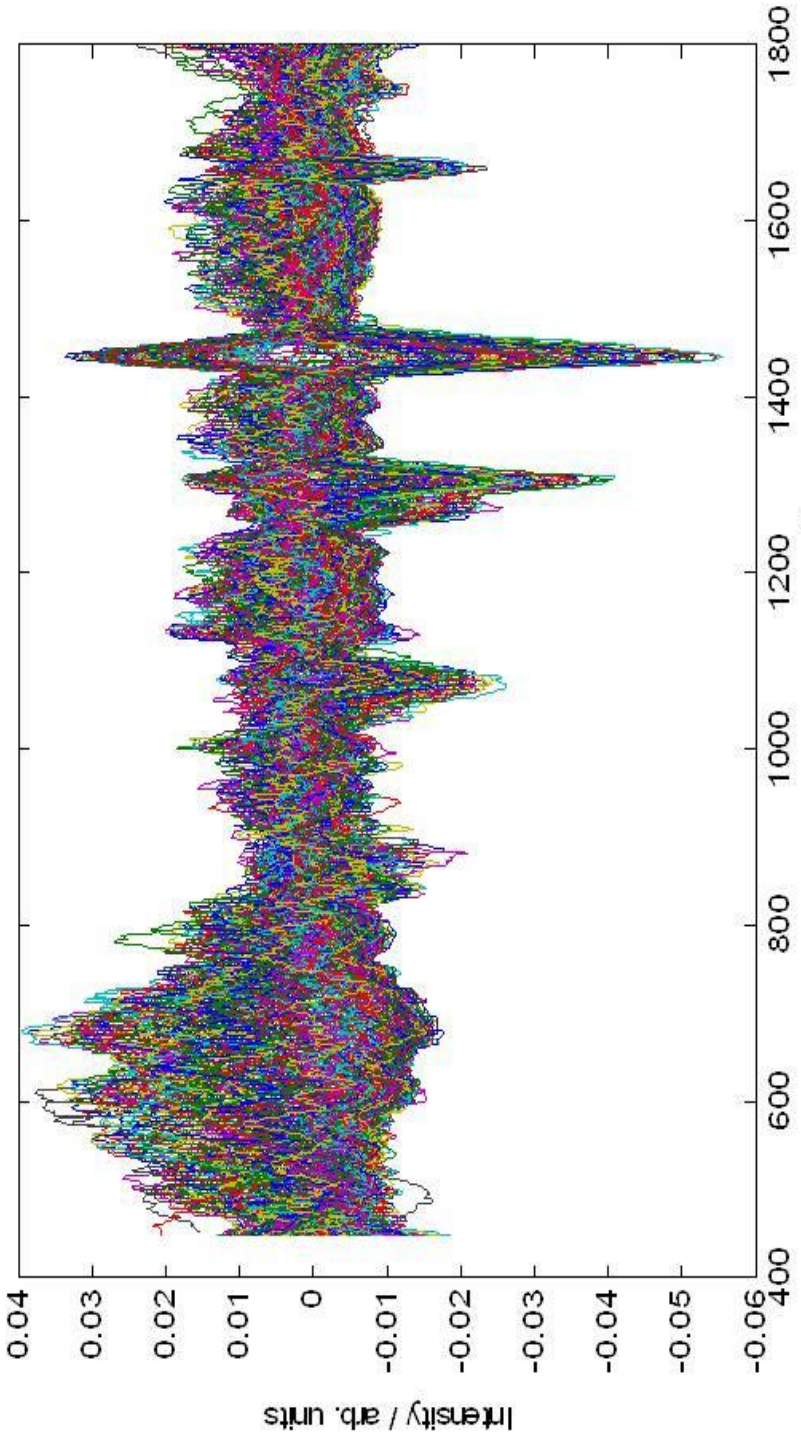

FIGURE 6.9 – Mean centred spectral data

FIGURE 6.10 – Principal Components for 6 Group model

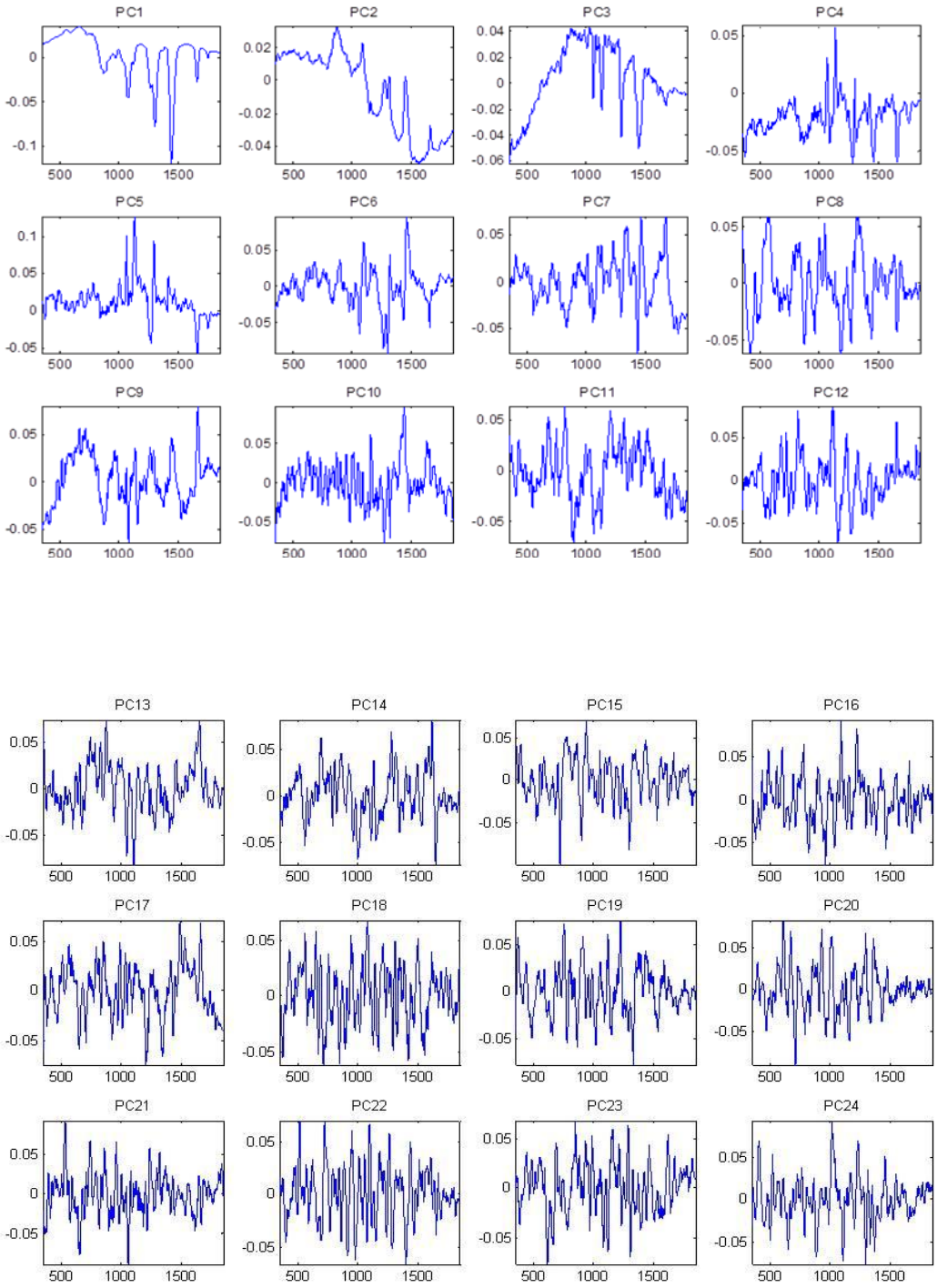

FIGURE 6.11 - Scatter plot demonstrating variation in 6 histological groups

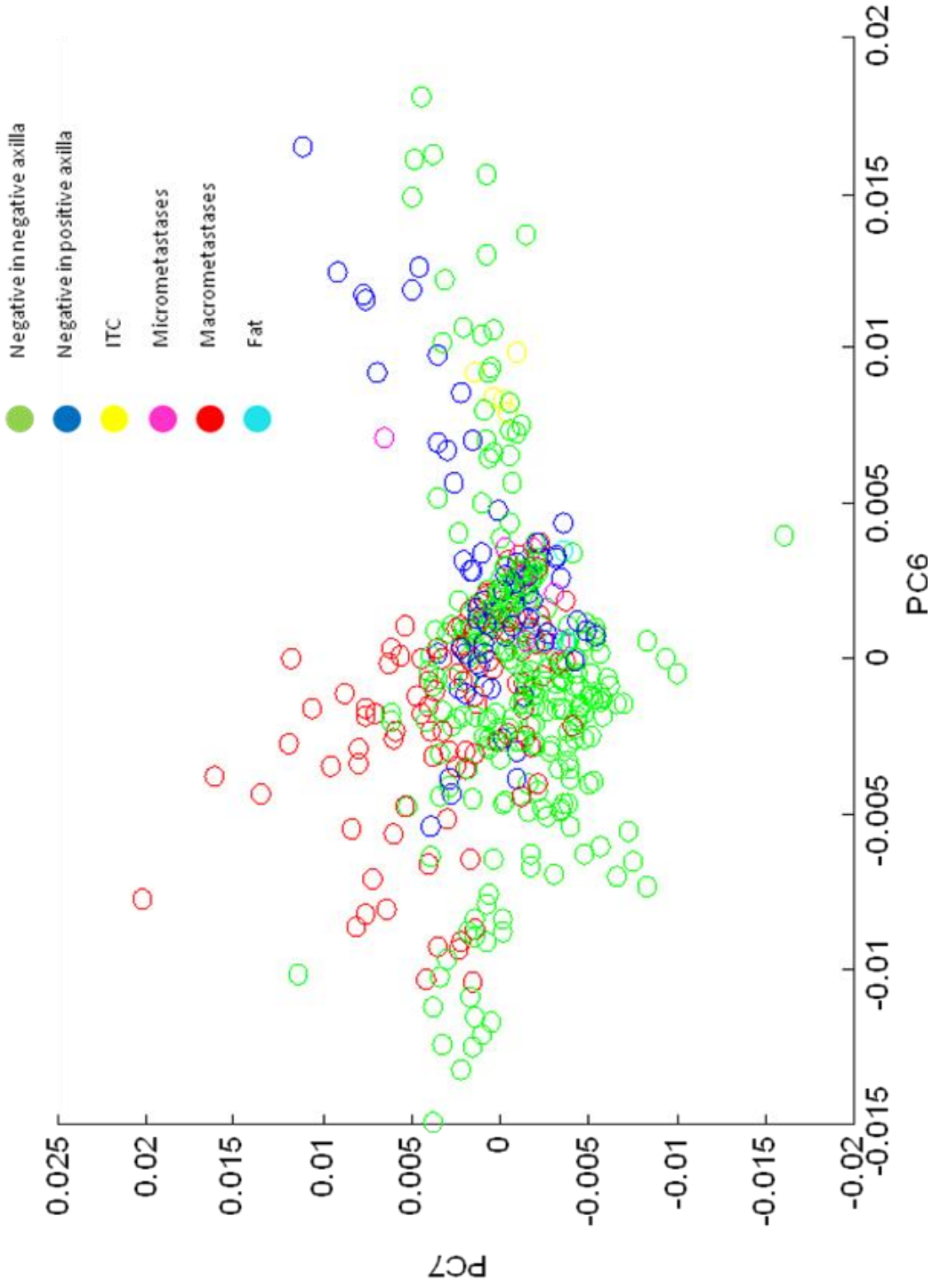

6.3.2 The "2 Group" Model

The "2 group" PC-LDA model is a more simplistic model which is more likely to reflect the clinical scenario of "malignant vs. benign". The training performance for this model is very much dependent on the data used for the malignant group and benign group. Predicted values are calculated from the Raman classification model.

For example:

If the benign group includes:

- *Negative nodes in negative axilla*
- *Negative nodes in positive axilla*

And the malignant group includes:

- *Macrometastases*
- *Micrometastases*
- *Isolated tumour cells*

	Predicted Benign	*Predicted Malignant*
Histologically Benign	*298*	*34*
Histologically Malignant	*36*	*81*

Overall training performance is 84.4%

Specificity is 90%

Sensitivity is 69%

However, the training model can in fact be improved by varying the components of the groups. Figure 6.11 demonstrates very few micrometastases and ITC within the results.

Furthermore, by inspecting the data, all of the micrometastases data were mispredicted. Whilst this is not in itself a valid reason to exclude the results, the tiny amount of spectra measured for this group means it has a disproportional effect on the overall results.

The optimal "2 group" model extrapolated from the data is shown below. Nodes containing ITC, fat and micrometastases were excluded due to their limited datasets as described above.

Benign group

- *Negative nodes in negative axilla*
- *Negative nodes in positive axilla*

Malignant group

- *Macrometastases*

Using this model, the principal components were calculated and ANOVA applied. The most significant PCs were once again found to be PC 6 and PC7 (Figure 6.12). The most prominent peaks emphasise the same differences in tissue concentration between benign and malignant groups as seen in the "6 group" model.

FIGURE 6.12 – PC6 and PC7 for 2 group model

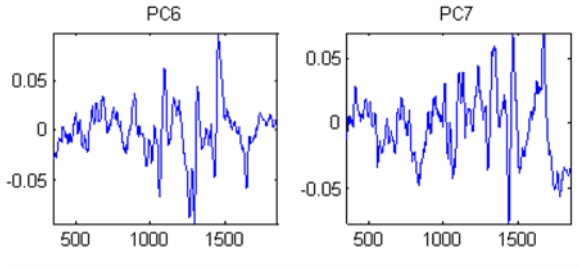

Figure 6.13 shows a good separation between the two groups although there is still a considerable degree of overlap. PC7 is developing more spread in the benign group but tightening up the malignant group. A plot of PC- LDA demonstrates this further in Figure 6.14.

The linear discriminant scores in the malignant group show a wide variation. This is likely to be a result of less malignant samples collected in comparison to benign samples (30 vs. 87 lymph node halves). This imbalance makes comparison of the 2 groups very difficult.

Cross validation of the datasets produce the following results:

	Predicted Benign	*Predicted Malignant*
Histologically Benign	*303*	*29*
Histologically Malignant	*30*	*74*

Overall training performance is 86.4%

Specificity is 91%

Sensitivity is 71%

FIGURE 6.13 – Scatter plot demonstrating separation between benign vs malignant nodes

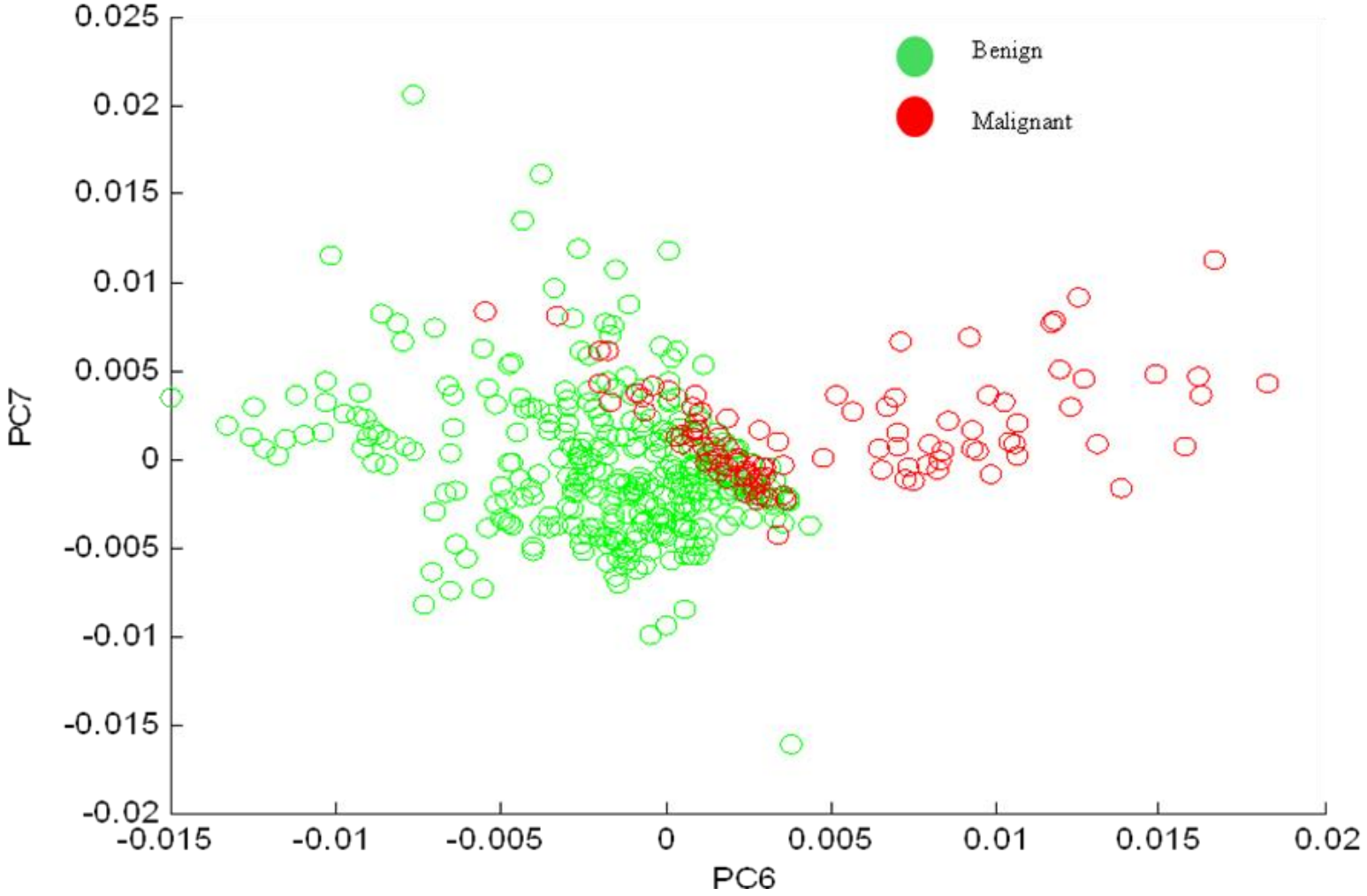

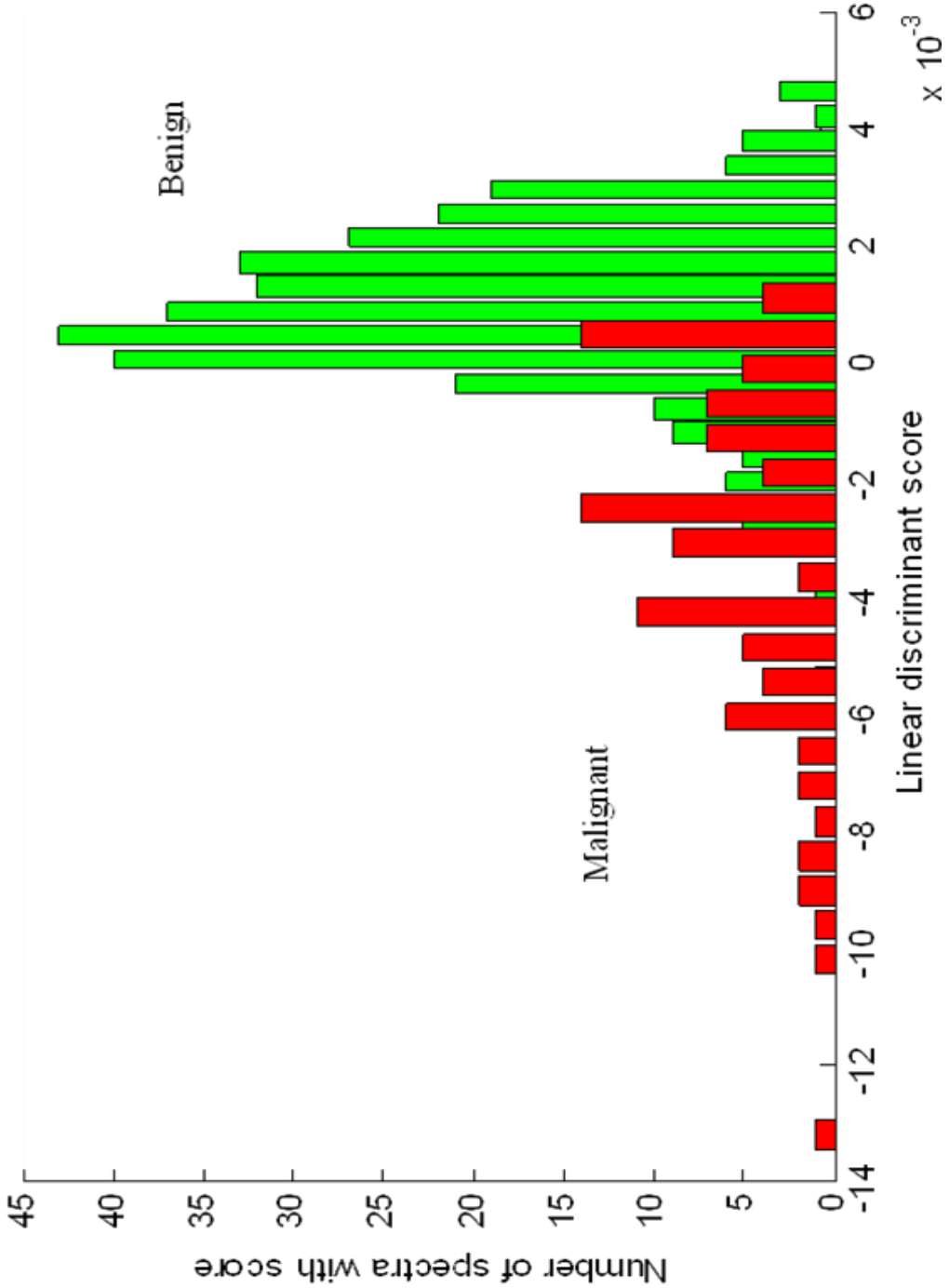

FIGURE 6.14 – Histogram demonstrating Linear Discriminant Analysis of Principal Components for comparison of benign vs malignant nodes

6.4 Sources of error

6.4.1 Surgical technique

Whilst the patients fell under the direct care of either of two consultants, the operations were occasionally carried out by surgical registrars under supervision as well as the consultants themselves. Fatty tissue around the resected lymph node, number of lymph nodes sampled and tissue damage would therefore have varied. In future studies, data collection could be limited to one consultant only, although the time taken to collect sufficient data would be longer. Alternatively, guidance could be given as to how best to harvest the nodes for spectral analysis such as fat removal and limited use of diathermy.

6.4.2 Probe efficacy

During the data collection period, the Raman probe (Probe A) broke and therefore failed to collect appropriate spectra on one of the collection days. A temporary replacement probe (Probe B) was provided before being switched back to the original Probe A once fixed. (Table 6.4). Figure 6.15 demonstrates the average spectra for the different probes. There does not appear to be any obvious changes with regards to intensity or Raman Shift.

Table 6.4 Patients affected by Probe changes

Patient number	Probe type
1-14	Probe A
15 - 30	Probe B
31-37	Probe A (fixed)

FIGURE 6.15 – Difference in the average spectra for probes used

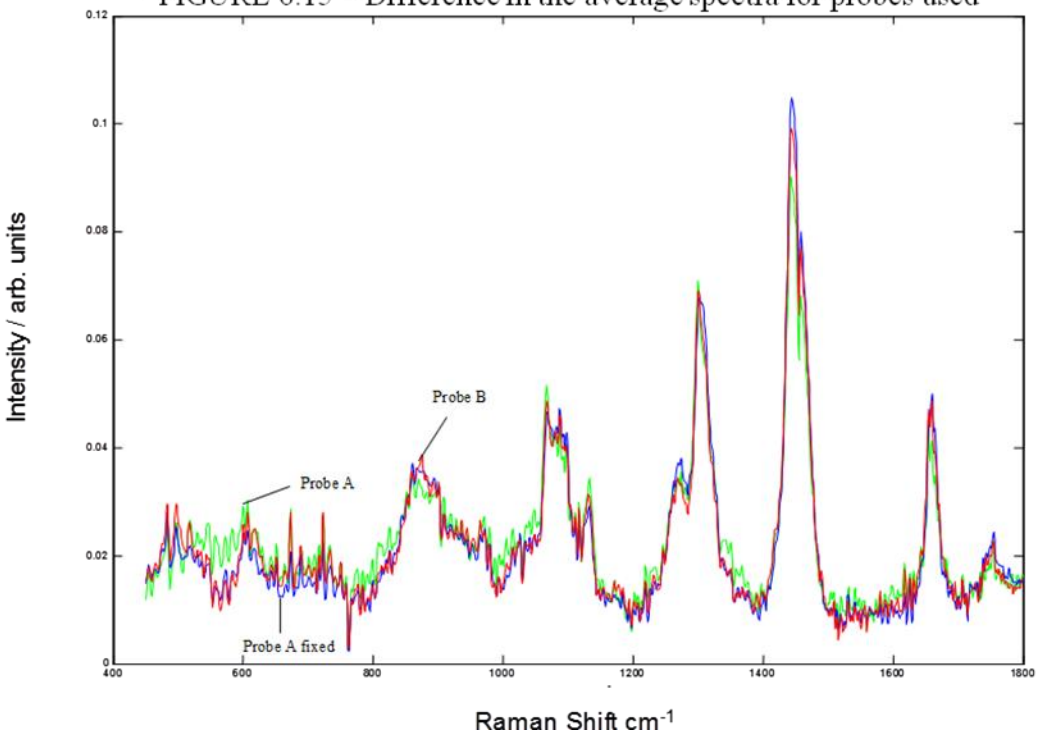

6.4.3 Blue dye

27 of the patients underwent sentinel lymph node biopsy and thus were injected with Patent Blue V dye pre-operatively around the areola of the ipsilateral breast. The remaining 10 patients underwent axillary node clearance.

Of these 27 patients, only 20 patients had nodes which were visibly blue despite the injection. Moreover, the degree of "blueness" varied considerably between samples as well as patients.

It was noted during collection of data that those lymph nodes with a strong blue colour were more likely to emit fluorescent spectra.

The measurement of the concentration of blue dye within each node and the effects on spectra collected was beyond the remit of this thesis. However, 2 laboratory based experiments were carried out to investigate the following hypotheses:

1) An increased concentration of blue dye in tissue causes fluorescence.

4 small cubes of raw chicken were prepared by soaking in the following solutions:

Chicken Sample	**Preparation**
Chick 1	Water only
Chick 2	25% Patent Blue V Dye solution
Chick 3	50% Patent Blue V Dye solution
Chick 4	75% Patent Blue V Dye solution

Each cube was then bisected and spectra collected with the handheld Raman Probe, using the same method as for the lymph node collection (Chapter 5).

Figure 6.16 demonstrates the average spectra for each chicken sample. It shows that an increased concentration of blue dye within the tissue elicits an increased fluorescence as well as a superimposed 'blue dye' Raman signal.

Figure 6.16 Average spectra recorded for each chicken sample

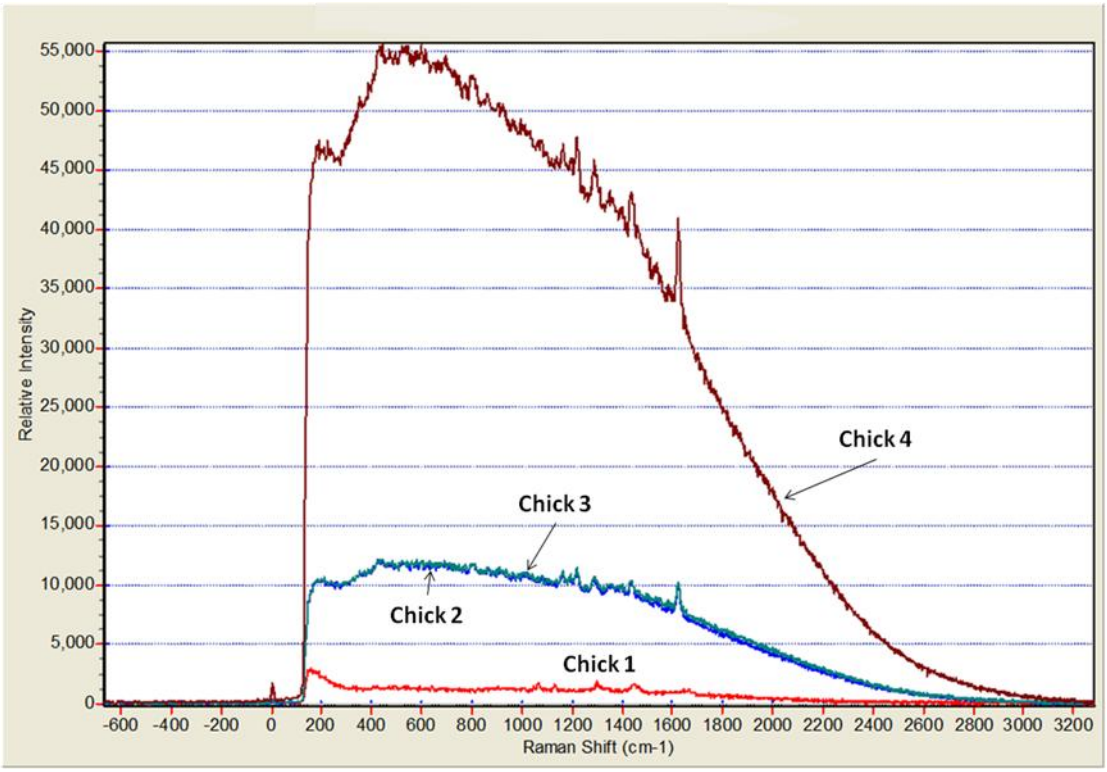

Figure 6.17 demonstrates the spectral intensity produced by blue dye alone in comparison to that produced by a single lymph node. The difference in intensity is such that it demonstrates how spectral measurements of lymph nodes might be skewed by its presence.

Figure 6.17 Spectral intensity produced by blue dye alone compared to a single lymph node

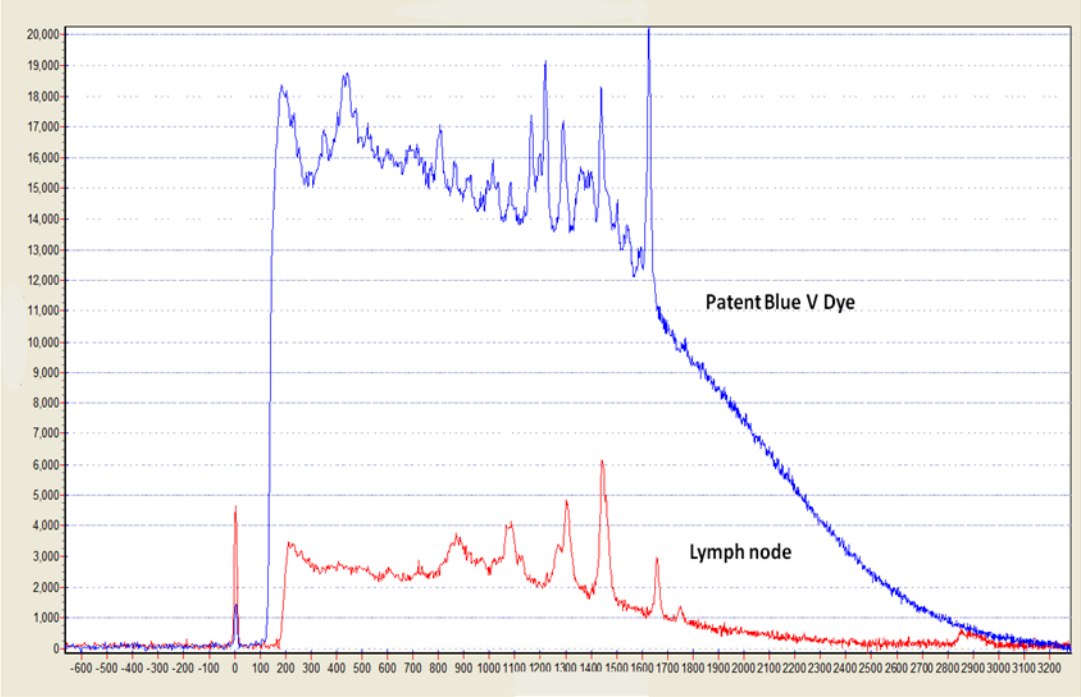

Figure 6.18 demonstrates the mean spectra for lymph nodes resected with visible blue dye infiltration compared to those with no visible blue dye. It emphasizes the difference in intensity of the signals as discussed previously. It should be noted that any significantly fluorescent data would have been rejected as part of the initial results analysis. Furthermore, although there appears to be an increase in background signal, the Raman peaks associated with the blue dye are not visible in either plot in Figure 6.18.

FIGURE 6.18 – Mean spectra for lymph nodes with visible blue dye vs no visible blue dye on resection

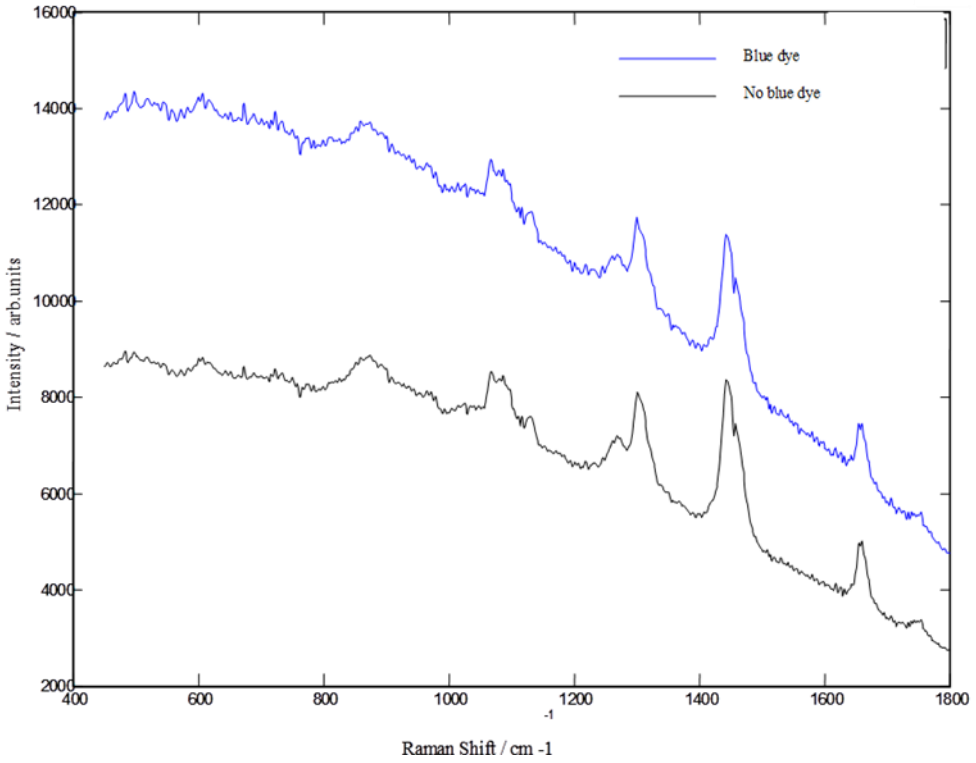

2) Spectral measurements of blue dye vary according to time exposed to light.

In order to assess whether spectra could have been related to factors such as exposure of blue dye to light once the vile was removed from its box or the length of time the blue dye was in the axilla, spectral measurements were taken of blue dye in the laboratory setting following varied exposure to light.

A vial of Patent Blue V dye was opened and pipetted into a sampling tube which was then sealed with glue. An initial spectra of the blue dye was collected, following the

same method described in Chapter 5. Thereafter spectra were collected at intervals of 40, 80, 120, 180 and 240 minutes and 23, and 24 hours. In between each set of measurements, the sampling tube was exposed to constant light.

No variation was seen in the spectra collected, suggesting that the blue dye was not affected by light exposure over the course of 24 hours.

6.4.4 Lymph node size

The size of the lymph nodes sampled varied considerably within and between patients. It was observed that the smaller the lymph node, the weaker the signal which is likely due to a reduced volume of tissue to measure. An increased likelihood of fluorescence was also noted which may be a result of an increased dye to tissue ratio, the effects of which are noted above.

CHAPTER 7 CONCLUSION

"Ah, but my effect will play a great role for chemistry and molecular structure."

C.V Raman

My research described in the preceding chapters has further investigated the role of Raman spectroscopy in the intraoperative assessment of lymph nodes in breast cancer management through interrogation of the molecular structure of both benign and malignant tissue. The work both complements and adds to the work done by Horsnell already (Horsnell *et al* 2010, 2012).

The first objective of this study was to assess the use of a hand-held Raman Spectroscopy probe in theatre as an accurate, rapid and non-destructive technique for intraoperative axillary node assessment. The methodology described in Chapter 5 was simple and could easily be followed by the surgeon or an attending non-clinician given the correct training. Although the time taken for spectral measurement was not formally recorded, the results were available within a reasonable time that would not delay the operation, which would otherwise increase anaesthetic time and delay the day's operating list.

The accuracy demonstrated by both the "6 group" and "2 group" training models, although not quite reaching the "gold standard" of post-operative histological analysis, is still

comparative to other techniques currently being researched for the clinical market. Frozen section has a similar sensitivity (57-74%) although specificity is far better (99-100%) (Layfield *et al* 2011). Similarly, cytology techniques have a sensitivity of 63% but again a far superior specificity rate (Tew *et al* 2005). Molecular techniques appear to be a better option than Raman spectroscopy but cost of set-up and logistics have already removed it from the market. According to Horsnell, the Raman probe system would only cost approximately £12000 (Horsnell *et al* 2010).

The other objective addressed in this study was whether the sensitivity of the Raman Spectroscopy probe is improved by recording spectra at more than one site on the lymph node. Horsnell quoted a sensitivity of up to 92% and a specificity of up to 99% in differentiating between normal and metastatic lymph nodes through measuring spectra at one single site of the lymph node. However, work done previously by Smith (Smith 2005) demonstrated that results for sensitivity and specificity were optimised when a greater number of sample blocks were collected from each node section. Unfortunately the "2 group" training model differentiating benign and metastatic lymph nodes produced both a lower specificity (91%) as well as sensitivity (71%). Reasons behind this disappointing figure might be multiple.

Firstly, due to time restraints and a broken probe, the amount of data collected was far less than in Horsnell's work. As discussed in Chapter 6, there was also a considerable imbalance in benign spectra collected compared with malignant spectra.

The data collection method may also have varied between studies. In Horsnell's work it is possible that each spectrum was only recorded if it demonstrated a good result, i.e. no evidence of poor signal or fluorescence. If the latter was the case then the lymph node could have been moved until a reasonable spectrum was achieved. However, the protocol in my methodology was perhaps more rigorous in that any spectra seen was recorded, thus replicating what would be expected in the clinical scenario. A significant number of spectra were therefore rejected prior to analysis, further reducing the pool of results to be analysed.

Furthermore, moving the lymph node at random around the probe, whilst increasing the area over which a micrometastasis or ITC might be found, may lead to missing spectra from a macrometastasis. Perhaps a more measured and controlled approach may have been beneficial.

The role of blue dye in creating increased fluorescence needs to be further investigated. However, the laboratory experiments using chicken cubes demonstrated that an increased concentration of blue dye within the tissue elicits increased fluorescence as well as

superimposed “blue dye” Raman signal. The number of lymph nodes with visible blue dye may well have varied between Horsnell’s work and my own work.

As well as approaching the above issues, the overall accuracy of the probe might be improved by development of a higher grade and more robust system. The probe might be redesigned so that it is able to sample a greater area of the lymph node to avoid the requirement for movement. It might also record a greater number of spectra whilst remaining a rapid assessment tool able to cope with the time limits of surgery. Other factors which might improve it are a better light source or better wavenumber resolution.

7.1 Future work

In deciding on future studies for the hand-held Raman Spectroscopy probe in breast cancer management, one must also consider where the clinical need lies. As mentioned in Chapter 1, Giuliano has argued that axillary dissection may not be necessary in all women with invasive breast cancer and sentinel node metastasis (Giuliano *et al* 2011), thus making the role of intraoperative lymph node assessment obsolete. However, the axillary nodes still need to be assessed and perhaps the role of the hand-held Raman probe as a non-invasive technique in the initial assessment clinic should be explored and promoted further.

Further work leading from this research may also include the use of a probe for:

- The assessment of calcifications picked up on mammograms
- The adequacy of local breast cancer resections with regards to tumour margins.
- Assessment of lymph nodes in lymphoma
- Assessment of lymph nodes where the primary cancer is unknown

BIBLIOGRAPHY

Alfano R, Liu C, Sha W, Zhu HR, Akins DL, Cleary J, Prudente R, Cellmer E. Human breast tissues studied by IR Fourier transform Raman spectroscopy. *Lasers in Life Science* 4 (1991): 23 - 28.

Association of Breast Surgery. Surgical guidelines for the management of breast cancer. *Association of Breast Surgery at BASO.* European Journal of Surgical Oncology, 2009.

Atkins, P., De Paula, J. *Physical Chemistry.* 9. Oxford: Oxford University Press, 2010.

Backus J, Laughlin T, Wang Y, Belly R, White R, Baden J, Justus Min C, Mannie A, Tafra L, Atkins D, Verbanac KM. Identification and characterization of optimal gene expression markers for detection of breast cancer metastasis. *Journal of Molecular Diagnostics* 7, no. 3 (August 2005): 327 - 336.

Baker R, Matousek P, Ronayne KL, Parker AW, Rogers K, Stone N. Depth profiling of calcifications in breast tissue using picosecond Kerr-gated Raman spectroscopy. *Analyst* 132, no. 1 (January 2007): 48 - 53.

Blumencranz P, Whitworth PW, Deck K, Rosenberg A, Reintgen D, Beitsch P, Chagpar A, Julian T, Saha S, Mamounas E, Giuliano A, Simmons R. Scientific Impact Recognition Award. Sentinel node staging for breast cancer: intraoperative molecular pathology overcomes conventional histologic sampling errors. *American Journal of Surgery* 194, no. 4 (October 2007): 426 - 432.

Boyle W, Smith G. Charge coupled semiconductor devices. *Bell System Technical Journal* (Bell Laboratories, Murray HIll, NJ) 49 (1970): 587 - 593.

Burkitt, Young, Heath. *Wheater's Functional Histology: A text and colour atlas.* 3. New York: Churchill Livingstone, 1993.

Conklin MW, Eickhoff JC, Riching KM, Pehlke CA, Eliceiri KW, Provenzano PP, Friedl A, Keely PJ. Aligned Collagen Is a Prognostic Signature for Survival in Human Breast Carcinoma. *American Journal of Pathology* 178, no. 3 (March 2011): 1221 - 1232.

Cox C, Centeno B, Dickson D, Clark J, Nicosia S, Dupont E, Greenberg H, Stowell N, White L, Patel J, Furman B, Cantor A, Hakam A, Ahmad N, Diaz N, King J. Accuracy of

intraoperative imprint cytology for sentinel lymph node evaluation in the treatment of breast carcinoma. *Cancer* 105, no. 1 (2005): 13 - 20.

Crow P, Molckovsky A, Stone N, Uff J, Wilson B, WongKeeSong LM. Assessment of fiberoptic near-infrared raman spectroscopy for diagnosis of bladder and prostate cancer. *Urology* 65, no. 6 (June 2005): 1126 - 1130.

Edge SB, Byrd DR, Compton CC. Breast. In *AJCC Cancer Staging Manual*, 347 - 376. New York: Springer, 2010.

Mbaye F, Fall M, Dem A, Sembene M. Biological evolution of tryptophan and phenylalanine in the occurence of breast cancer in Senegalese women. *International Journal of Medicine and Medical Sciences* 4, no. 4 (April 2012): 103-109.

Frank CJ, McCreery RL, Redd DC, Gansler TS. Detection of Silicone in Lymph Node Biopsy Specimens by Near-Infrared Raman Spectroscopy . *Applied Spectroscopy* 47, no. 4 (1993): 387 - 390.

Giuliano AE, Hunt KK, Ballman KV, Beitsch PD, Whitworth PW, Blumencranz PW, Leitch AM, Saha S, McCall LM, Morrow M. Axillary dissection vs no axillary dissection in women with invasive breast cancer and sentinel node metastasis: a randomized clinical trial. *Journal of American Medical Association*, February 2011: 569 - 575.

Haka AS, Shafer-Peltier K, Fitzmaurice M, Crowe J, Dasari RR, Feld MS. Diagnosing breast cancer by using Raman spectroscopy. *Proceedings of the National Academy of Sciences USA* 102, no. 35 (August 2005): 12371 - 12376.

Haka AS, Shafer-Peltier KE, Fitzmaurice M, Crowe J, Dasari RR, Feld MS. Identifying microcalcifications in benign and malignant breast lesions by probing differences in their chemical composition using Raman spectroscopy. *Cancer Research* 62, no. 18 (September 2002): 5375 - 5380.

Hanlon EB, Manoharan R, Koo TW, Shafer KE, Motz JT, Fitzmaurice M, Kramer JR, Itzkan I, Dasari RR, Feld MS. Prospects for in vivo Raman spectroscopy. *Physics in Medicine and Biology* 45, no. 2 (February 2000): R1 - 59.

Harris AT, Rennie A, Waqar-Uddin H, Wheatley SR, Ghosh SK, Martin-Hirsch DP, Fisher SE, High AS, Kirkham J, Upile T. Raman spectroscopy in head and neck cancer. *Head and Neck Oncology* 5, no. 2 (October 2010): 26.

Haybittle JL, Blamey RW, Elston CW, Johnson J, Doyle PJ, Campbell FC, Nicholson RI, Griffiths K. A prognostic index in primary breast cancer. *British Journal of Cancer* 45, no. 3 (March 1982): 361 - 366.

Herzberg G. *Molecular spectra and molecular structure vol.II: Infrared and Raman spectra of polyatomic molecules.* Vol. 2. New York: Van Nostrand Reinhold, 1945.

Horsnell J, Stonelake P, Christie-Brown J, Shetty G, Hutchings J, Kendall C, Stone N Raman spectroscopy--a new method for the intra-operative assessment of axillary lymph nodes. *Analyst.* 135, no. 12 (December 2010): 3042 - 7.

Horsnell J The use of Raman Spectroscopy for the intraoperative assessment of axillary nodes in breast cancer. *PhD Thesis*. Cranfield University 2012

Ioachim HL, Rathech H. *Ioachim's lymph node pathology*. 3. Lippincott Williams and Wilkins, 2002.

Isabelle M, Stone N, Barr H, Vipond M, Shepherd N, Rogers K. Lymph node pathology using optical spectroscopy in cancer diagnostics. *Spectroscopy* 22, no. 2 (2008): 97 - 104.

Kast R, Serhatkulu G, Cao A, Pandya A, Dai H, Thakur J, Naik V, Naik R, Klein M, Auner G, Rabah R. Raman spectroscopy can differentiate malignant tumours from normal breast tissue and detect early neoplastic changes in a mouse model. *Biopolymers* 89 (2008): 235 - 241.

Kendall C. A study of Raman spectroscopy for the early detection and classification of malignancy in oesophageal tissue. *PhD Thesis,* School of Engineering, Cranfield University, 2002.

Kendall C, Isabelle M, Bazant-Hegemark F, Hutchings J, Orr L, Babar J, Baker R, Stone N. Vibrational spectroscopy: a clinical tool for cancer diagnostics. *Analyst* 134 (2009): 1029 - 1045.

Kendall C., Hutchings J, Barr H, Shepherd N, Stone N. Exploiting the diagnostic potential of biomolecular fingerprinting with vibrational spectroscopy. *Faraday Discussions* 149 (2011): 279 - 290.

Kneipp J, Bakker Schut T, Kliffen M, Menke-Pluijmers M, Puppels G. Characterization of breast duct epithelia: a Raman spectroscopic study. *Vibrational Spectroscopy* 32, no. 1 (2003): 67 - 74.

Layfield DM, Agrawal A, Roche H, Cutress RI. Intraoperative assessment of sentinel lymph nodes in breast cancer. *British Journal of Surgery* 98, no. 1 (January 2011): 4 - 17.

Leikola JP, Toivonen TS, Krogerus LA, von Smitten KA, Leidenius MH. Rapid immunohistochemistry enhances the intraoperative diagnosis of sentinel lymph node metastases in invasive lobular breast carcinoma. *Cancer* 104, no. 1 (July 2005): 14 - 19.

Liu YL, Qian HX, Qin L, Zhou XJ, Zhang B, Chen X. Association of serum lipid profile with distant metastasis in breast cancer patients. *Zhonghua Zhong Liu Za Zhi. Chinese.* 34, no. 2 (Feb 2012): 129-31.

Liu, Q. Role of optical spectroscopy using endogenous contrasts in clinical cancer diagnosis. *World Journal of Clinical Oncology* 2, no. 1 (January 2011): 50 - 63.

Loftus P. Doctors thought J&J cancer test was impractical. *Wall Street Journal*, January 2010.

Maiman T. Stimulates optical radiation in ruby. *Nature* 187 (1960): 493 - 494.

Manoharan R, Shafer K, Perelman L, Wu J, Chen K, Deinum G, Fitzmaurice M, Myles J, Crowe J, Dasari RR, Feld MS. Raman spectroscopy and fluorescence photon migration for breast cancer diagnosis and imaging. *Photochemistry and Photobiology* 67, no. 1 (January 1998): 15 - 22.

McClure W, Davis A. Fast Fourier Transforms in the Analysis of Near-Infrared Spectra. In *Analytical Applications of Spectroscopy*, by Davies A Creaser C, 414 - 436. London: Royal Society of Chemistry, 1988.

Molckovsky A., Wong Kee Song L-M, Shim MG, Marcon NE, Wilson BC. Diagnostic potential of near-infrared Raman spectroscopy in the colon: differentiating adenomatous from hyperplastic polyps. *Gastrointestinal Endoscopy* 57, no. 3 (March 2003): 396 - 402.

Montgomery E, Bronner MP, Goldblum JR, Greenson JK, Haber MM, Hart J, Lamps LW, Lauwers GY, Lazenby AJ, Lewin DN, Robert ME, Toledano AY, Shyr Y, Washington K. Reproducibility of the diagnosis of dysplasia in Barrett esophagus: a reaffirmation. *Human pathology* 32, no. 4 (April 2001): 368 - 378.

Office for National Statistics. *Registrations of cancer diagnosed in 2008, England.* Cancer Statistics Registrations, Series MB1 no.39, London: National Statistics, 2010.

Opel M, Venturini F. Raman scattering in solids. *European Pharmaceutical Review* 7, no. 3 (2002): 76.

Raman CV, Krishnan KS. A new type of secondary radiation. *Nature* 121 (1928): 501 - 502.

Rehman S, Movasaghi Z, Tucker A, Joel P, Darr J, Ruban A, Rehman I. Raman spectroscopic analysis of breast cancer tissues: identifying differences between normal, invasive ductal carcinoma and ductal carcinoma in situ of the breast tissue. *Journal of Raman Spectroscopy* 38, no. 10 (October 2007): 1345 - 1351.

Salem AA, Douglas-Jones AG, Sweetland HM, Mansel RE. Intraoperative evaluation of axillary sentinel lymph nodes using touch imprint cytology and immunohistochemistry. Part II. Results. *European Journal of Surgical Oncology* 32, no. 5 (June 2006): 484 - 487.

Shafer-Peltier KE, Haka AS, Fitzmaurice M, Crowe J, Myles J, Dasari R, Feld MS. Raman microspectroscopic model of human breast tissue: implications for breast cancer diagnosis in vivo. *Journal of Raman Spectroscopy* 33, no. 7 (July 2002): 552 - 563.

Sharkey FE, Greiner AS. Morphologic identity of primary tumour and axillary metastasis in breast carcinoma. *Archives of Pathological Laboratory Medicine* 109 (1985): 256 - 259.

Shetty G, Kendall C, Shepherd N, Stone N, Barr H. Raman spectroscopy: elucidation of biochemical changes in carcinogenesis of oesophagus. *British Journal of Cancer* 94, no. 10 (May 2006): 1460 - 1464.

Shim M, Wilson B, Marple E, Wach M. Study of fiber-optic probes for in vivo medical Raman spectroscopy. *Applied Spectroscopy* 53, no. 6 (1999): 619.

Siebert, F., Hildebrandt, P. *Vibrational spectroscopy in life science.* Weinheim: Wiley, 2008.

Smith J, Kendall C, Sammon A, Christie-Brown J, Stone N. Raman spectral mapping in the assessment of axillary lymph nodes in breast cancer. *Technology in cancer research and treatment* 2, no. 4 (August 2003): 327 - 332.

Smith J, Kendall C, Sammon AM, Christie-Brown J, Mandalia T, Stone N. Raman spectroscopy is sensitive and specific in the detection of lymph node metastases in breast cancer. *Progress in Biomedical Optics and Imaging - Proceedings of SPIE* 5862 (2005): 1 - 7.

Smith J. Raman Spectroscopy in the assessment of lymph nodes in breast cancer. *PhD Thesis.* Cranfield University, 2005.

Stone N, Baker R, Rogers K, Parker AW, Matousek P. Subsurface probing of calcifications with spatially offset Raman spectroscopy (SORS): future possibilities for the diagnosis of breast cancer. *Analyst* 132, no. 9 (2007): 899 - 905.

Stone N., Matousek P. Advanced transmission Raman spectroscopy: a promising tool for breast disease diagnosis. *Cancer Research* 68, no. 11 (June 2008): 4424 - 4430.

Stone, N., Kerssens M, Rhys Lloyd G, Faulds K, Graham D, Matousek P. Surface enhanced spatially offset Raman spectroscopic (SESORS) imaging – the next dimension. *Chemical Science* 2, no. 4 (2011): 776 - 780.

Tew K, Irwiq L, Matthews A, Crowe P, Macaskill P. Meta-analysis of sentinel node imprint cytology in breast cancer. *British Journal of Surgery* 92, no. 9 (September 2005): 1068 - 80.

Thakur J, Dai H, Serhatkulu G, Naik R, Naik V, Cao A, Pandya A, Auner G, Rabah R, Klein M, Freeman C. Raman spectral signatures of mouse mammary tissue and associated lymph nodes: normal, tumour and mastitis. *Journal of Raman Spectroscopy* 38 (2007): 127 - 134.

University of Cambridge. *Raman Spectroscopy*. October 2007. http://www.doitpoms.ac.uk/tlplib/raman/index.php (accessed May 2012).

UK Trial of Early Detection of Breast Cancer Group. 16-year mortality from breast cancer in the UK Trial of Early Detection of Breast Cancer. *Lancet* 353, no. 9168 (1999):1909-14.

Veronesi U, Paganelli G, Galimberti V, Viale G, Zurrida S, Bedoni M, Costa A, de Cicco C, Geraghty JG, Luini A, Sacchini V, Veronesi P. Sentinel-node biopsy to avoid axillary dissection in breast cancer with clinically negative lymph nodes. *Lancet* 349, no. 9069 (June 1997): 1864 - 7.

APPENDIX A

A summary of the TNM classification system for breast derived from the AJCC cancer staging manual (Edge SB 2010):

Primary tumour (T)

TX: Primary tumour cannot be assessed.

T0: No evidence of primary tumour.

Tis: Carcinoma in situ (DCIS, LCIS, or Paget disease of the nipple with no associated tumour mass)

T1 (includes T1a, T1b, and T1c)**:** Tumour is 2 cm or less in diameter

T2: Tumour is between 2 cm and 5 cm in diameter

T3: Tumour is more than 5 cm in diameter

T4: Tumour of any size growing into the chest wall or skin. This includes inflammatory breast cancer.

Lymph Node (N)

NX: Nearby lymph nodes cannot be assessed (for example, removed previously).

N0: Cancer has not spread to nearby lymph nodes.

- **N0 (i+):** Tiny amounts of cancer are found in axillary lymph nodes using immunohistochemistry. The area of cancer spread contains less than 200 cells and is less than 0.2 mm.
- **N0 (mol+):** Cancer cells cannot be seen in axillary lymph nodes, but traces of cancer cells were detected using PCR.

N1: Cancer has spread to 1 to 3 axillary lymph node(s), and/or tiny amounts of cancer are found in internal mammary lymph nodes on sentinel lymph node biopsy.

- **N1mi:** Micrometastases in 1 to 3 axillary lymph nodes.
- **N1a:** Macrometastases in 1 to 3 axillary lymph nodes.

- **N1b:** Metastases to internal mammary lymph nodes found specifically during sentinel lymph node biopsy but not clinically enlarged.
- **N1c**: Both N1a and N1b apply.

N2: Cancer has spread to 4 to 9 axillary lymph nodes or cancer has enlarged the internal mammary lymph nodes (either N2a or N2b, but not both).

- **N2a:** Micrometastases to 4 to 9 axillary lymph nodes
- **N2b:** Metastases to one or more internal mammary lymph nodes, causing them to become enlarged clinically.

N3: Any of the following:

- **N3a:** either
  - Macrometastases to 10 or more axillary lymph nodes OR
  - Macrometastases to the infraclavicular lymph nodes
- **N3b:** either:
  - Macrometastases in at least one axillary lymph node with enlargement of the internal mammary lymph nodes, OR
  - Macrometastases in 4 or more axillary lymph nodes and metastases in internal mammary lymph nodes on sentinel lymph node biopsy.
- **N3c:** Macrometastases to the supraclavicular lymph nodes.

Metastasis (M):

MX: Presence metastasis cannot be assessed.

M0: No distant spread is found on x-rays (or other imaging procedures) or by physical exam.

- **cM0 (i +):** Small numbers of cancer cells are found in blood or bone marrow (found only by special tests), or micrometastases are found in lymph nodes away from the breast.

M1: Metastatic spread to distant organs is present, the most common sites being bone, lung, brain, and liver.